Research Paper

Mixed Convection Heat Transfer Characteristics of Al_2O_3 – MWCNT Hybrid Nanofluid under Thermally Developing Flow; Effects of Particles Percentage Weight Composition

Ibrahim Umar Ibrahim [a,b], Mohsen Sharifpur [a,c,d,*], Josua P. Meyer [a,e]

[a] Department of Mechanical and Aeronautical Engineering, University of Pretoria, Pretoria 0002, South Africa
[b] Department of Mechanical Engineering, Ahmadu Bello University Zaria, Kaduna State, Nigeria
[c] School of Mechanical, Industrial and Aeronautical Engineering, University of the Witwatersrand, Private Bag 3, Wits 2050, South Africa
[d] Department of Medical Research, China Medical University Hospital, China Medical University, Taichung, Taiwan
[e] Department of Mechanical and Mechatronic Engineering, Stellenbosch University, Stellenbosch, South Africa

ARTICLE INFO

ABSTRACT

In this research, an experimental investigation of hybrid nanofluid mixed convection heat transfer characteristics is conducted. The research specifically investigates the effects of percentage weight composition (PWC) of nanoparticles in the hybrid nanofluids on mixed convection heat transfer characteristics along the lamina, transition and turbulent regions. Transition boundaries, thermal entrance effects, and the influence of tube axial position were also critically investigated and analysed experimentally. Three hybrid nanofluids of Al_2O_3 – MWCNT (i.e., Al_2O_3 (60%) – MWCNT (40%), Al_2O_3 (50%) – MWCNT (50%) and Al_2O_3 (40%) – MWCNT (60%)) were prepared using two-step method and then subjected to a constant heat flux through a horizontal circular copper tube with an internal diameter of 8mm. Results show a significant change in heat transfer characteristics with different PWCs. Al_2O_3 (60%) – MWCNT (40%) have shown a better heat transfer enhancement among the three fluids investigated. Its Nusselt number has an enhancement of more than 5 % better than the other two fluids. Along the transition regime, critical Reynold numbers (Re_{cr}) of the three nanofluids were found to have differed slightly, with Re_{cr} = 2020, 2000 and 2100 for Al_2O_3 (60%) – MWCNT (40%), Al_2O_3 (50%) – MWCNT (50%) and Al_2O_3 (40%) – MWCNT (60%) respectively. Mixed convection effects were found to be more significant with Al_2O_3 (60%) – MWCNT (40%) than with the other two fluids. At the axial position of 63.75, its mixed convection strength (Ω) was about 41%, which is the highest among the three fluids. Its strength of mixed convection was also found to deteriorate to about 14.75% with an increase in axial distance from the tube inlet. A similar observation was also noticed with other fluids. Thermal entrance effects were only found to be significant at x/d = 15 and 31.25, as their influence diminishes with an increased x/d distance from the tube inlet. It was concluded that both mixed convection and thermal entrance effects resulted in heat transfer enhancement, especially in the lamina region. Their influences decrease with an increase in axial distance from the tube inlet. Mixed convection influences were only present in the lamina and transition region, and their strength was reduced with an increase in Reynold number and axial position.

1. Introduction

Hybrid nanofluids are advanced heat transfer fluids with improved heat transfer characteristics and better thermo physical properties than single nanofluids and other convectional working fluids [1–3]. With the recent advancements in science and technology, the thermal management of new advanced advice has become a great challenge and an obstacle to their performance and operation efficiency. Therefore, these fluids are believed to play an important role in the future thermal management of these new devices. However, to properly utilize their full potential, we mustfully understand their properties and performance characteristics. Research findings from the literature have shown that hybrid nanofluids' force convective heat transfer characteristics differ significantly from those of single nanofluids [4]. Hybrid nanofluid heat transfer characteristics also differed when the percentage weight

Nomenclature

A	Constants
As	Surface Area [m2]
c_{bf}	Specific heat capacity of base [J/kgK]
c_{hnf}	Specific heat capacity of Hybrid [J/kgK]
c_p	Specific heat capacity of Particles [J/kgK]
D_{si}	Internal Tube diameter [m]
D_{so}	Outer Tube Diameter [m]
g	Acceleration due to gravity
Gr	Grashof Number
Gz	Graetz Number
$h(x)$	Local Heat transfer coefficient [W/m2K]
h_{avg}	Average Coefficient of Heat transfer [W/m2K]
I	Current [A]
j	Colburn J Factor
k	Thermal Conductivity [W/Mk]
k_{cu}	Thermal conductivity of the copper [W/Mk]
L	Test Section Length [m]
$\dot{m}$	Mass flow Rate [kg/s]
$Nu(x)$	Local Nusselt Number
Nu_{avg}	Average Nusselt Number
P	Perimeter of the tube [m]
Pr	Prandtl Number
$\dot{Q_e}$	Electric Energy Supply Rate [W]
$\dot{q_{in}}$	Heat flux [W/m2]
$\dot{Q_f}$	Heat Transfer Rate [W]
Ra	Raleigh Number
Re	Reynold Number
Ri	Richardson Number
R_{cr}	Critical Reynold number
T_a	Ambient Temperature [oC]
T_i	Inlet Temperature [oC]
$T_f(x)$	Local Mean Fluid Temperature [oC]
$T_{si}(x)$	Inside wall temperature [oC]

$T_{so}(x)$	Outside wall temperature [oC]
V	Voltage [V]
x	Distance from the tube inlet [m]

Greek Letters

ρ_{hnf}	Density of the Hybrid nanofluids [kg/m3]
ρ_{bf}	Base fluid density [kg/m3]
ρ_p	Density of Particles [kg/m3]
μ	Viscosity [kg/m.s]
υ	Kinematic viscosity [m2/s]
ρ	Density [kg/m3]
φ	Volume concentration

Subscripts

b	Bulk
w	Wall
p	Particles
o	Outlet/Out
i	Inlet
f	Fluid
s	Surface
a	Ambient/ Atmospheric
avg	Average
cr	Critical
hnf	Hybrid nanofluids
bf	Base fluid.
P	Particles
β	Coefficient of Thermal expansion
Φ	Free convection effects
Ω	Heat transfer Parameter (another form of Nusselt number)

Abbreviations

PWC	Percentage weight compositions
HTC	Heat Transfer coefficient
HNF	Hybrid Nanofluid
UWT	Uniform wall temperature
UHF	Uniform Heat flux

compositions (PWC) of the nanoparticles in the hybrid mixture varied [5]. This was due to the significant influence of PWC on the fluids' (i.e., HNF) properties. Among the notable properties that were reported to be affected by the variation of the PWC are viscosity and thermal conductivity [6]. These properties significantly influenced the heat transfer characteristics [7]. Therefore, it is paramount to investigate these effects on the heat transfer characteristics. However, despite their promising prospects, a lot remains to be learned about their properties and characteristics. Research work by Hussien et al. [8] and Suresh et al. [4] has shown a significant improvement in forced convective heat transfer performance with hybrid nanofluids than with single or mono nanofluids. Giwa et al. [9] findings show that percentage weight compositions, volume concentration, and particle sizes significantly influence the hybrid nanofluid heat transfer characteristics. Those aspects identified by the work of Giwa et al. [9] significantly affected the force convective heat transfer characteristics of hybrid nanofluids, more especially PWC. Research findings by Ramadhan et al [5] and Hameed et al. [10–11] have also reaffirmed the influence of the percentage weight composition of nanoparticles in the hybrid nanofluid mixture. However, the effects of this aspect (i.e., PWC) was not investigated in the transition region. Table 1 shows the summary of the important research studies using nanofluids in the transition region. Finding shows that no research investigated the transition characteristics of hybrid nanofluids. Despite the fact that the transition region have a very short range, some research findings have shown that there is a high tendency of having an

improve heat transfer characteristics within the region. The region was largely neglected due to inadequate information, high uncertainty and unreliability that makes flow predictions uncertain [12]. To date very little was known about the hybrid nanofluid characteristics in the region. This can also be seen from Table 1, that no research investigates the heat transfer characteristics of these advance fluids in the region. Research findings from the work of Everts et al. [13] and Ghajar et al. [14] have shown that transition boundary can be effected by several factors. These factors includes working fluid characteristics, tube orientations, inlet configurations, roughness of the tube, applied heat flux, etc. Still none of these aspects were investigated with hybrid nanofluids. Therefore this research, aimed at investigating the effects of hybrid nanofluid PWC on the transition boundary conditions.

One of the critical reasons for developing new heat transfer fluids like nanofluids is to have a working fluid that can perform better in all conditions, for effective and efficient thermal management. However, it is essential to note that, at high heat flux, there is a tendency for free convection. Which has implications on fluid characteristics, especially heat transfer. Natural convection or free convection in tube flow is normally caused by buoyancy-induced secondary flow [22]. Buoyancy effects can often be so strong that they can be compared to forced convection, especially in practical scenarios where systems operate at a low flow rate and at a significant heat dissipation rate [23]. It is important to note that buoyant force direction in relation to the main fluid flow is critical to mixed convection heat transfer characteristics. It

was found that natural convection presence in a tube may enhance or deteriorate the fluid's force convective heat transfer performance. Because it all depends on the direction of the buoyant forces in relation to the direction of the main fluid flow. Oliver et al. [24] explained that natural convection enhanced the convective heat transfer coefficient in flow instances where forced fluid motion and buoyancy-induced motion are in the same direction. However, buoyancy reduces the heat transfer rate if they are in the opposite direction. Oliver et al. [24] also explain that natural convection influence in the laminar region is often very strong and may even enhance the heat transfer performance by a factor of approximately three to four above the prediction from analytical correlations. The same was also explained by Bergles et al. [25]. Conditions, where natural convection exists with forced convection heat transfer, are regarded as mixed convection [26]. The presence of secondary flows may result in thermal stratification, the formation of rotating vortices, and increasing fluid pressure. It may also enhance heat transmission, shorten thermal entrance length, and cause an early transition to turbulent flow [27]. Despite the significance of this phenomenon on heat transfer characteristics of working fluids, there is very little experimental data on mixed convection heat transfer characteristics of hybrid nanofluids. Especially when compared to what is available with other working fluids (i.e., ethylene glycol, water, etc.). Table 2 shows that no experimental research yet investigates and characterizes hybrid nanofluid mixed convection heat transfer. Research has shown that, due to nanofluids distinctive properties and characteristics, not all research findings with other working fluids would apply to them [28]. Therefore, it is imperative to investigate and adequately characterise their mixed convection heat transfer phenomena.

In an experimental research study, Feng et al. [29] investigate the mixed convection laminar heat transfer of silicon oxide nanofluid. Water and ethylene glycol (EG) were used as base fluid in a ratio of (50:50). Findings show that experimental Nusselt numbers were much higher than the predicted values by empirical correlation. This was attributed to the presence of natural convection influences. Variation of fluid viscosity and its effects on mixed convection has also been discussed by Shome et al. [27]. He explained that underestimating viscosity's effects on mixed convection is unrealistic; doing so may result in a significant error. The reason is that most fluid viscosity varies significantly even at moderate wall-to-fluid temperature gradients. Moreover, this issue of viscosity is very concerning, especially with nanofluids. Research has shown that their viscosity is affected by different parameters. For instance, a review work by Mahbubul et al. [30] reported that particle size significantly affects nanofluid viscosity. In the literature, it was also widely reported that their viscosity reduces when the fluid temperature rises [31]. Understandably, nanofluid viscosity is affected by many factors. Most of these factors are peculiar to nanofluids alone. Factors like particle sizes, volume concentration, particle density, type of base fluids, etc. [31–34]. These varied characteristics influence their heat transfer performances, so they tend to behave differently from other heat transfer fluids. Therefore, it is important to understand these fluids fully and their characteristics under different conditions.

Derakhshan et al. [35] investigate the mixed convection heat transfer characteristics of multi-walled carbon nanotubes (MWCNT) using inclined, horizontal, and fin tubes. Results show that the Nusselt number was enhanced significantly when the volume concentration increased at a particular Grashof number. Findings show that under aided flow circumstances, increasing the Grashof number boosted the heat transfer coefficient in the horizontal tube. Nevertheless, with the increase in tube inclination angle and Richardson number, the effect of nanoparticles on heat transfer enhancement diminishes. Additionally, the effect of volume concentration is more pronounced in the smooth tube than in the micro-fin tube. Ben Mansour et al. [36] insistent that there is a need for more research on the mixed convection effects on nanofluid heat transfer rates, citing the discrepancies that exist between the numerical studies and the very few experimental works available. Some numerical studies, particularly those of Ben Mansour et al. [37] and Khanafer et al. [38], demonstrate that nanofluid natural convection heat transfer increases as particle concentration rises. On the other hand, experimental results [39] clearly show the opposite trend. This shows the wide gap that exists in the literature. Therefore, this research aims to bridge the gap in the literature by investigating and characterising the mixed convection heat transfer of hybrid nanofluids. Due to the nature and uniqueness of the hybrid nanofluids, this research, as a first step, will focus on investigating the effects of varying nanoparticle weight percentage composition (PWC) in the hybrid mixture. Also, the research considered both the lamina, transition and turbulent regions. Rather than just one flow regime. The literature survey (i.e., Table 2) shows that no research was done that investigated and characterized hybrid nanofluid force convection or mixed convection heat transfer in the transition region. The few studies that are available on mixed convections were limited to the lamina region, and they involved only single nanofluids [29,40].

Another important aspect considered in this research is the importance of axial positions and their influence on heat transfer

Table 1

Summary of Relevant experimental Studies on Convective Heat Transfer of Nanofluids in The Transition Region

Reference	Tube	Base Fluid	particles sizes	Vol. Conc.	Reynold No. Range	Type of Nanofluid	Key findings
Meyer et al. [15]	Circular tube	Water	MWCNT (OD:10-20 nm and L: 10-30um)	0.33, 0.75, and 1.0%	1000 -7000	Single	Nanofluid viscosity increased significantly, while the Nu also increased by about 33.2%.
Chougule and Sahu [16]	Circular tube	Water	Al_2O_3 (<100 nm)	0.15	2400-4000	Single	Nanofluid performance was enhanced to about 37.5%.
Osman et al. [17]	Rectangular tube	Water	Al_2O_3 (-)	0.3, 0.5, and 1 %	200 -7000	Single	The most notable development in heat transfer was 54% in the transition regime, with just about an 11% increase in the turbulent power at 0.1% concentration.
Sharma et al. [18]	Circular tube	Water	Al_2O_3 (47 nm)	0.02 and 0.1 %	3000-9000	Single	At Re = 9000 and a concentration of 0.1%, an enhancement of HTC of ~ 23.7% was reported.
Yang et al. [19]	Circular tube	ATF	Graphite (20–40 nm)	2wt.%	0- 120	Single	HTC was found to have lower values than predicted by the correlations for homogeneous fluids or the conventional heat transfer correlations for heterogeneous fluids.
Ma et al.[20]	Circular tube	Water	Fe_2O_3 (-)	0.16 %, 0.05%, and 0.24%	2400 -3200	Single	A systematic drop in HTC with increasing nanoparticle concentrations in the transition regime was observed.
Naik et al. [21]	Circular tube	Water	CuO (50 nm)	0.025, 0.5, and 0.1 %	2500-10000	Single	Nu values have increased to about 5.4 times with the helical inserts of 3.0 twist ratio, while the plain tube improves by about 28% at 0.5% of CuO.

characteristics. This aspect of heat transfer together with thermal entrance effects were not been investigated with hybrid nanofluids. Because of their importance, they were also investigated and characterised in this research. Most of the research findings in the literature did not consider the effects of thermal entrance on heat transfer characteristics. This aspect was largely neglected in the nanofluids literature. Research findings by Everts et al. [50] using water show that thermal entrance effects are often more significant in the lamina region than in the other regions. Thermal entrance effects are often more dominant at axial positions that are very close to the tube inlet. Ghajar et al. [51] and Everts et al. [50] suggested that at such tube positions (i.e., close to the tube inlet), enhancement of heat transfer was largely due to the thermal entrance effects rather than mixed convection. These two phenomena (i.e., mixed convection and thermal entrance) were often misunderstood and hardly differentiated. Therefore, in this research, both the thermal entrance effects, mixed convection effects, and the influence of axial position on hybrid nanofluid characteristics were thoroughly investigated, characterised, and differentiated.

2. Nanofluid preparation

2.1. Preparation of Al_2O_3 – MWCNT hybrid nanofluids

The nanoparticles used in this study were bought from Nano Research Materials Inc. (USA) and used without any modifications. They have the following physical data and properties, as given in Table 3.

To investigate the effects of percentage weight compositions (PWC) on this hybrid nanofluid. Three hybrid fluid nanofluids were prepared using a two-step method. Nanofluids prepared are Al_2O_3 (60%) – MWCNT (40%), Al_2O_3 (50%) – MWCNT (50%) and Al_2O_3 (40%) – MWCNT (60%). To prepare a nanofluid with Al_2O_3 (60%) and MWCNT (40%). Al_2O_3 and MWCNT nanoparticles were weighted and dispersed in deionised water (DI – Water) using a ratio of 60:40. To improve the fluid stability, Sodium Dodecylbenzene Sulfonate (SDBS) surfactant was

Table 2
Summary of experimental studies on convective heat transfer of hybrid nanofluids

References	Flow Regime	Base Fluid	Nanoparticles Used	Preparation Method	Concentration (vol.%)	Enhancement /Remark
Ramadhan et al. [5]	Turbulent	EG/Water	TiO_2–SiO_2	One-step method	1%	The 40:60 mixture ratio gives the highest enhancement of about 36%, while 50:50 has the lowest enhancement.
Suresh et al. [4]	Laminar	Water	Al_2O_3–Cu	two-step method	0.1%	An enhancement of about 14% was recorded at Re=1730. Al_2O_3-DI water nanofluids have lower friction than Al_2O_3–Cu/DI water nanofluids.
Syam et al. [41]	Turbulent	Water	CNT - Fe_3O_4	two-step method	0.1 – 0.5%	31.10% increment was recorded for the plain tube while 42.51% with twisted tape inserts at a Re = 22000. Pumping power was found to increase about 1.18 times.
Balaji et al. [42]	Laminar	Water	GNP- MWCNT	two-step method	0.01 – 0.2%	The convective HTC of nanofluid increased up to 85%.
Hameed et al. [10]	Laminar	Water	Al_2O_3–Cu and Al_2O_3 -MWCNT	two-step method	0.1, 0.3	Al_2O_3–MWCN/water hybrid has a better enhancement of HTC of about 30.65%, while the Al_2O_3–Cu/water has an enhancement of approximately 20.48% at the same concentration of 0.3.
Shahsavar et al.[43]	Laminar	Water	Fe_2O_3 - CNT	two-step method	0.5 -0.9%	Fe_3O_4-MWCNT nanofluid shows better enhancement with the magnetic field (constant) than the alternating magnetic field without magnetic field excitations. An improvement of about 62.7% Nu was recorded at 0.5 % loading and Re = 2190.
Gupta et al. [44]	Laminar	Water	Zn-Fe_2O_4	two-step method	0.02 – 0.5	The HTC was improved to about 42.99% at 0.5 concentration.
Naddaf et al. [45]	Laminar	Diesel's oil	Gr- MWCNT	two-step method	0.05–0.5	The HTC of the fluid increases with the increase of the fluid velocity at all weight concentrations. It shows that using nanoparticles improves heat transfer more than the friction factor.
Hussien et al. [46]	Laminar	Water	GNP- MWCNT	two-step method	0.075–0.125	Findings show that the pressure drops rise by about 12.4%, while entropy generations drop by about 37.5% in the micro tubes for the hybrid nanofluid.
Hussien et al. [8]	Laminar	Water	MWCNTs/GNPs	two-step method	0.075–0.25 wt%	The heat transfer characteristics were highly improved using MWCNT and MWCNT- GNPs hybrid fluids. Adding GNPs to the MWCNT has proven vital as it significantly increases the heat transfer performance to about 43.4%, while the pressure drops only rise to a maximum of 11.0% compared to the water.
Megatif et al. [47]		Water	TiO_2–CNT	modified hydrolysis technique	0.1–0.2 wt.%	Significant improvement of the heat transfer characteristics was reported at 0.2 wt. %.
Gupta et al. [48]	Laminar	Water	Ag-MWCNT	two-step method	0.02–0.5 mass%	59.8% enhancement was obtained with the hybrid nanofluid of Ag-MWCT, while 67.5% was observed with MWCNT-distil water.
Hameed et al. [11]	Turbulent	Water	Al_2O_3-CNT	two-step method	0,1, 0,3	Nu increased with an average value of 15.41% for 0.1% concentrations and an average value of 22.11% for 0.3%, compared to the plain tube with water. Also, the friction factor has the highest increment of 39.82% in the turbulent flow regime with 0.3.
Mohammad et al.[49]	Laminar, transient, and turbulent	Water	Fe_2O_3 - CNT	two-step method	0.1% and 0.2%	Results showed that the hybrid nanofluid of Fe_2O_3-MWCNT has the most significant heat transfer improvement compared to the base fluid. At 0.1 concentration, there is an increase in heat transfer by 13.54% and 27.69 % along the laminar and turbulent flow regimes, respectively.

Table 3

Summary of nanoparticles used and their physical properties

Nanoparticles	Particle sizes[nm]	Purity [%]	Specific heat [J/kg K]	Thermal conductivity[W/mK]
Al$_2$O$_3$	20	99	880	37
MWCNT	30-50	95	711	3000

Source: Material data sheets from Nano Research Materials Inc. (USA), (US4314) and Li et al. [52]

added. The mixture was then subjected to magnetic Stirring for 30 minutes. It was then later followed by an ultra-sonication process for one hour at an amplitude of 90. This was to break any particle agglomerations and properly disperse the nanoparticles in the base fluid. Anoop et al. [53] and Nadooshan et al. [54] also used a similar approach. The fluid temperature was controlled at 20°C using a thermal bath during the sonication process.

The same approach was followed to prepare the other two fluids, Al$_2$O$_3$ (50%) – MWCNT (50%) and Al$_2$O$_3$ (40%) – MWCNT (60%).

The density and heat capacity (specific) of the hybrid nanoparticles of Al$_2$O$_3$ – MWCNT were calculated using equation (1) and equation (2) as given by [55–56].

$$\rho_{(Al_2O_3-MWCNT)} = \frac{\left(\rho_{(Al_2O_3)}PWC_{(Al_2O_3)}\right) + \left(\rho_{(MWCNT)}PWC_{(MWCNT)}\right)}{\left(PWC_{(Al_2O_3)} + PWC_{(MWCNT)}\right)} \tag{1}$$

$$c_{(Al_2O_3-MWCNT)} = \frac{\left(c_{(Al_2O_3)}PWC_{(Al_2O_3)}\right) + \left(c_{(MWCNT)}PWC_{(MWCNT)}\right)}{\left(PWC_{(Al_2O_3)} + PWC_{(MWCNT)}\right)} \tag{2}$$

Specific heat capacity and density of the Al$_2$O$_3$ – MWCNT hybrid nanofluids were estimated from the following mixture rules in equations (3) and (4), which were widely used in the literature, such as Naik et al. [21].

$$\rho_{hnf} = (1-\varphi)\rho_{bf} + \varphi\rho_p \tag{3}$$

$$c_{hnf} = (1-\varphi)c_{bf} + \varphi c_p \tag{4}$$

Where ρ_{hnf} c_{hnf} φ ρ_{bf} c_{bf} c_p and ρ_p are the hybrid nanofluids density, heat capacity (specific), concentrations, base fluid density (DI water), the specific heat capacity of the DI water (base fluid), the specific heat capacity of the hybrid nanoparticles, and the density of the hybrid nanoparticles.
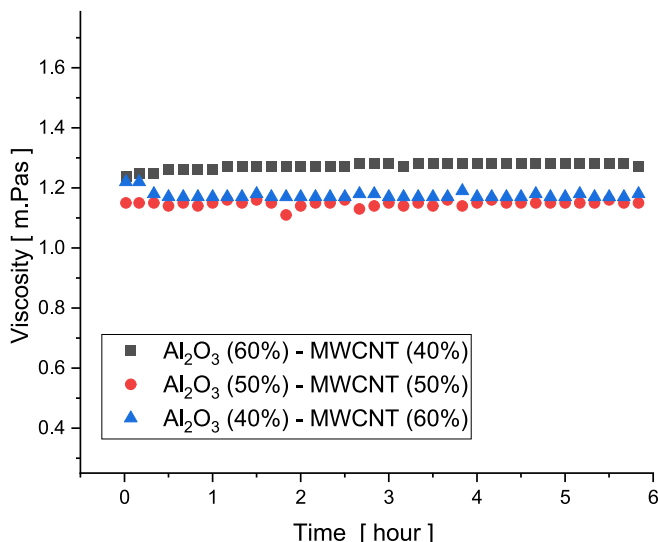
2.2. Stability and thermo physical properties of the hybrid nanofluids

A viscosity measuring meter (SV–10 vibro viscometer A&D, Japan) was used to measure and monitor the fluid's viscosity and to examine the stability of the nanofluids. Viscosity readings were taken at a constant temperature of 25°C, as indicated in Figure 1. The device is programmed to record and login data at an interval of 10 minutes for about six hours. Osman et al. [17] and Giwa et al. [57–58] also used a similar approach. Nanofluids were also visually monitored for ten days, and no sign of agglomeration or sedimentation was noticed. These show that the nanofluids prepared have satisfactory stability. Six hours (i.e., 6 hours) were chosen because it takes roughly 3 to 3.5 hours to complete the experiments.

2.2.1. Thermal conductivity

Figure 2 shows the thermal conductivity of the hybrid nanofluids measured using a KD2 Pro thermal conductivity meter at different temperatures between 10°C and 30°C. Measurements were taken within an error limit of less than 0.1. The thermal conductivity of the hybrid nanofluid varied with a change in nanoparticle percentage weight composition. Al$_2$O$_3$ (40%) – MWCNT (60%) have shown higher thermal conductivity values, while Al$_2$O$_3$ (60%) – MWCNT (40%) have the lowest thermal conductivity.

2.2.2. Viscosity of the hybrid nanofluid

See Figure 3. Shows the viscosity of the hybrid nanofluids measured using Sv–10 Vibro Viscometer (A&D, Japan), which has an uncertainty of less than 3% when operating at full capacity.

Results show that hybrid nanofluid viscosity also varied with changes in percentage weight composition (PWC). It has already been demonstrated that nanofluid viscosity decreases with increased temperature [3]. This agrees with our research findings, as fluid viscosity decreased with temperature rise.

3. Experimental setup and test section

3.1. Experimental setup

Figure 4 shows the basic design of the experimental setup. The Force convection test setup consists of a storage tank (8) that can store and supply 10 litres of nanofluid for use during testing. A magnetic gear pump with variable speed (1). The power supply was attached to the test section, which creates a consistent heat flux along the heat exchanger and heats the fluid from T_i to T_o . The test section was well insulated with insulation material, with a thickness of about 70mm and six layers. This was to prevent heat loss to the surroundings. The fluid left the test
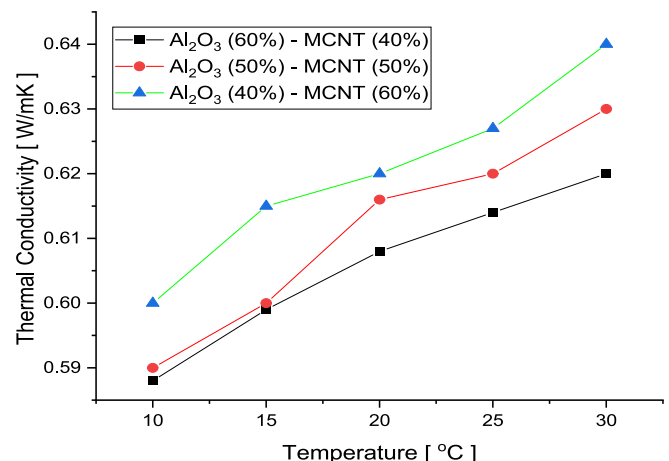

Figure 1. Stability checking at 25°C for 6hr.

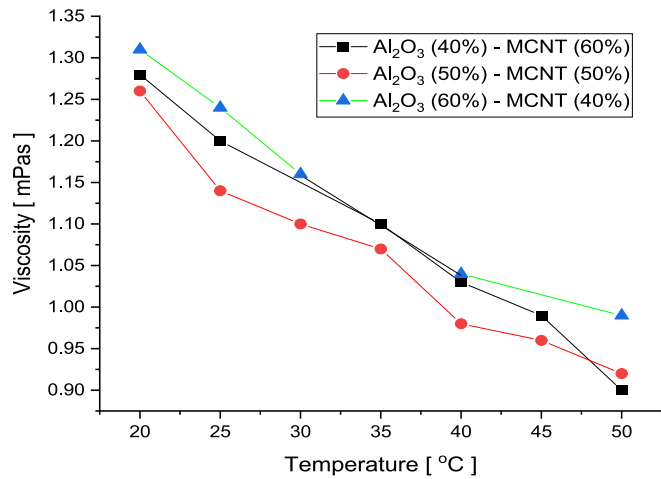**Figure 2.** Thermal conductivity of the hybrid nanofluids

Figure 3. Viscosity of hybrid nanofluids

section through the Coriolis flow meter (CmFs015), which, when operating at full scale, had a 0.05% accuracy. This flow meter ranges from 0.204kg/min to 4.09kg/min (4). A heat exchanger (5) was used to cool the hot fluid (i.e., fluid heated from the test sections (3)). The heat was then absorbed by water from a thermal bath (6), and the temperature at the inlet of the test section was kept constant.

The system was equipped with a data-capturing device that collects information/signals from the power supply, flow meters, thermocouples, etc., and processes them with the aid of a computer (9). Data was logged using a Lab view application (2014 version) designed to log in data at a frequency of 20 Hz. 200 readings were captured and then averaged for analysis for every single data point.

3.2. Test section

The test section used in this study is depicted in Figure 5 and comprises two mixers (i.e., at the inlet and outlet). Heat transfer section (i.e., Heat exchanger), and a 500 mm hydrodynamic entrance section. The entrance section or hydrodynamic length of the test section was calculated based on the correlation given by Dust et al. [59], as presented in Equation (5). Because of limited space on the experimental setup, the

design was based on the Reynold of 1700, which resulted in L/D = 96.00 and the maximum hydrodynamic entrance of 500mm. This was in accordance with the work of Meyer et al. [15].

$$\frac{L}{D} = \left[(0.619)^{1.6} + (0.0567 \text{Re})^{1.6} \right]^{\frac{1}{1.6}} \tag{5}$$

The heated part of the test sections is made from a copper tube material with a wall thickness of about 1 mm. The tube has internal and external diameters of 8.00 mm and 9.50mm, respectively. The length of the test section is 1000mm. 28 T-type thermocouples were evenly positioned throughout the test section wall at seven thermocouple positions. Each position has four thermocouples measuring the wall temperature. These thermocouples were placed on the copper tube at 120, 250, 380, 510, 640, 770, and 900mm from the tube inlet. A tiny pilot hole was drilled into the test section to fix the thermocouples, followed by a drop of solder, which was used to fasten the thermocouple securely on the tube. A gap of about 1mm between the thermocouple's position and the tightly coiled Constantine wire was kept to maintain a constant supply of heat flux without interfering with thermocouple readings. A similar approach was also maintained in the work of Evert et al. [13]. Two T-type thermocouples, which record the inlet and outlet temperatures, were also situated at the tube inlet and outlet.

All 30 thermocouples were calibrated to within the accuracy of 0.1 °C, between the temperatures of 10 to 60°C, using a constant temperature thermal bath.

A Constantine heating wire was used to heat the test section at 217.8 W using a DC power supply at 180 V and a current supply of 1.21 A.

3.3. Experimental procedure

The experimental procedure was explained in [56] but will be briefly narrated here for clarity. Firstly, before readings are taken, the system is required to be stabilised. This takes about 90 minutes after starting up before it reaches steady-state condition. When there are no discernible temperature and flow rate changes, a steady state is thought to have been reached. Little adjustments were introduced to the fluid mass flow rates to achieve the desired new flow rate for data recordings after the system had attained a steady state. It takes around 10 minutes for the system to recover to its steady state for any adjustment in mass flow rate made (i.e., from a higher flow rate to a lower flow rate). To avoid any
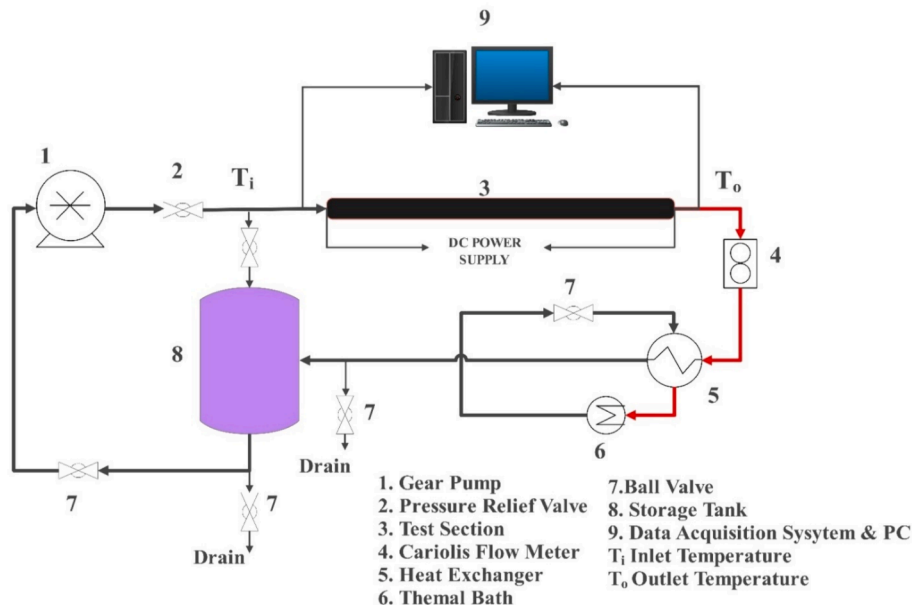

Figure 4. Schematics Diagram of the Test Section

residual heat being retained in the insulation and distorting the subsequent measurement, data were collected from the high flow rate to the lower flow rate. For each data point, 200 readings were taken by the data acquisition systems and then averaged for analysis.

3.4. Data analysis and validation

3.4.1. Heat transfer

The data analysis method used in this research is similar to the method followed by Meyer et al. [15], and it was also explained in Ibrahim et al. [56]. However, for clarity, we presented it here as follows.

The fluid heat transfer $h(x)$ coefficient obtained from the relation,

$$h(x) = \frac{\dot{q}_{in}}{T_{si}(x) - T_f(x)} \tag{6}$$

Where $\dot{q}_{in}$ is the heat flux computed from the heat transfer rate.$\dot{Q}_f$

$$\dot{q}_{in} = \frac{\dot{Q}_f}{A_s} \tag{7}$$

The rate of heat transfer to the fluid $\dot{Q}_f$ is computed from equation (8)

$$\dot{Q}_f = \dot{m}c_p(T_{out} - T_{in}) \tag{8}$$

A_s is the tube's internal surface area.

$$A_s = \pi D L \tag{9}$$

Supplied energy

$$Q_e = VI \tag{10}$$

The local inner surface temperatures $T_{si}(x)$ and $T_f(x)$ were calculated using outer wall temperature, $T_{so}(x)$ and resistance through the tube wall R_w, as shown below. This was also explained by Ibrahim et al. [56].

$$T_{si}(x) = T_{so}(x) - \dot{q}_{in}R_w \tag{11}$$

Where.

$$R_w = \frac{\ln\frac{D_{so}}{D_{si}}}{2\pi k_{cu}L} \tag{12}$$

k_{cu} the copper tube thermal conductivity was calculated as in the work by Abu-Eishah et al. [60] and Meyer et al. [15]. T_f which is defined as fluid local mean temperature was computed from the relation given in equation (13) [15].

$$T_f(x) = T_i + \frac{\dot{q}_{in}xp}{\dot{m}c_p} \tag{13}$$

Where;

p is the perimeter of the copper tube.

The coefficient of convective heat transfer (Average)h_{avg} was determined by averaging the preceding equation (6) along the tube length at all seven thermocouple points. Thus, by averaging the convective coefficient of heat transfer $h(x)$ (local) at all thermocouple locations.

$$h_{avg} = \frac{(h(x_1) + h(x_2) + h(x_3) + \ldots\ldots h(x_n))}{n} \tag{14}$$

Where,

n = 7.

Hybrid nanofluids, Reynold, and Prandtl numbers were obtained from equations (15) and (16).

Reynold number Re

$$Re = \frac{4\dot{m}}{\pi D L} \tag{15}$$

Prandtl number Pr.

$$Pr = \frac{\mu c_p}{k} \tag{16}$$

The average Nusselt number was obtained from h_{avg} given in equation (14).

$$Nu_{avg} = \frac{h_{avg}D}{k} \tag{17}$$

k represent the fluid's thermal conductivity. For water, thermal conductivity was determined using the correlation developed by Popiel et al. [61] at fluid bulk temperature T_b.

Nanofluid thermal conductivity was estimated at bulk temperature using the correlations of Pak and Cho [62] given in equation (18). The viscosity of the hybrid nanofluid was determined at bulk temperature using a regression equation (19). This was in accordance with the method used by Sharma et al. [18], Osman et al. [17], and Ibrahim et al. [56].

$$k_{nf} = k_w(1 + 7.47\varphi) \tag{18}$$

$$\mu_{nf} = \mu_w(1 + 2.5\varphi + 6.2\varphi^2) \tag{19}$$

$$j = \frac{Nu}{RePr^{\frac{1}{3}}} \tag{20}$$

3.4.2. Mixed convection analysis

Graez and Grashof numbers are evaluated from equations (21) and (22), respectively.

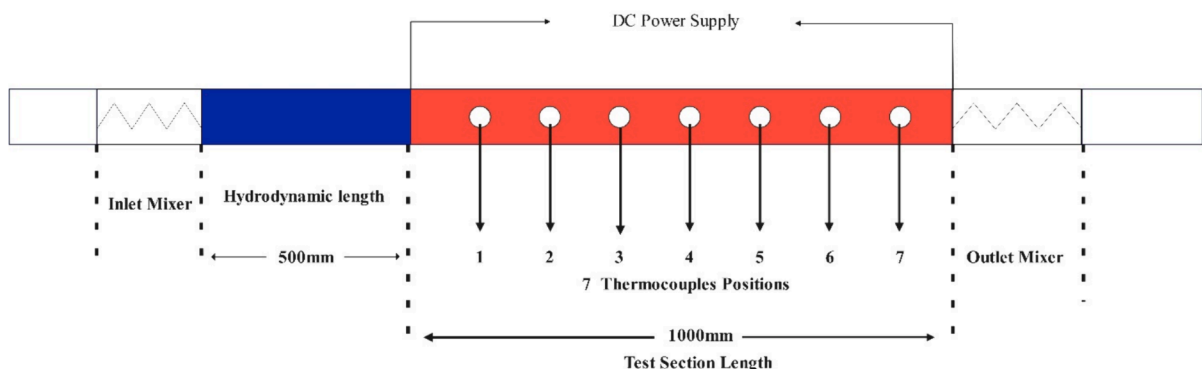$$Gz = \frac{\pi}{4}RePr\frac{D}{L} \tag{21}$$

Figure 5. Schematic diagram of the test section

$$Gr = \frac{g\beta(T_s - T_m)D^3}{v^2} \tag{22}$$

Rayleigh number from equation (23)

$$Ra = GrPr \tag{23}$$

Richardson number Ri

$$Ri = \frac{Gr}{Re^2} \tag{24}$$

To analyse the effects of natural convection on the hybrid nanofluids, a similar analysis from the work of Feng et al. [29] is adopted.

The simplified average Nusselt number relation is presented in equation (25).

$$Nu_F\left(\frac{\mu_w}{\mu_b}\right)^{0.14} = \begin{cases} 1.75Gz^{\frac{1}{3}}.............(UWT) \\ 2.11Gz^{\frac{1}{3}}.............(UHF) \end{cases} \tag{25}$$

The two equations provided above are for the two conditions, Uniform wall temperature condition (UWT) and Uniform heat flux conditions (UHF), while the Gz is summarized as.

$$Gz \geq 26.2\left(RePr\frac{D}{L} \geq 33.3\right) \tag{26}$$

The term $\left(\frac{\mu_w}{\mu_b}\right)^{0.14}$ represents the radial viscosity variation in the tube, as suggested by [27]. The influence of natural convection cannot be ignored when there is a significant temperature difference or heat flux. Consequently, efforts have been made to correlate any deviations from the aforementioned relation [24,63,64].

$$Nu\left(\frac{\mu_w}{\mu_b}\right)^{0.14} = A(Gz + \Phi)^{\frac{1}{3}} \tag{27}$$

Moreover, the parameter Ȩ́ can be correlated to the Prandtl, Grashof, and Graetz numbers, which are expressed in equation (28).

$$\Phi = \left[\frac{1}{2.11}Nu\left(\frac{\mu_w}{\mu_b}\right)^{0.14}\right]^3 - Gz \tag{28}$$

The parameter Φ or $\frac{\Phi}{Gz}$ measures the impact of natural convection on heat transfer. The greater the value of Φ or $\frac{\Phi}{Gz}$, the greater the importance of free convection.

Feng et al. [29] and Yang et al. [19] explained that it's more appropriate and convenient to analyse the influence of mixed convection on the Reynold number and Nusselt number if the results are presented in terms of a parameter Ω, which is given in equation (29).

$$\Omega = Nu\left(\frac{\mu_w}{\mu_b}\right)^{0.14}\left(Pr\frac{D}{L}\right)^{-\frac{1}{3}} \tag{29}$$

From equations (29) and (21), we rewrite equation (25) as presented in equation (30) [19].

$$\Omega_F = Nu\left(\frac{\mu_w}{\mu_b}\right)^{0.14}\left(Pr\frac{D}{L}\right)^{-\frac{1}{3}} = 2.11\left(Re\frac{\pi}{4}\right)^{\frac{1}{3}} = 1.95Re^{-\frac{1}{3}} \tag{30}$$

Therefore, in this study, equation (30) will be used as the datum or baseline to which the effect of natural convection will be measured or assessed. The higher the data deviate from equation (30) (i.e., the data point above equation (30), the more significant the natural convection effects are. This is in accordance with the work of Yang et al. [19].

3.5. Validations of experimental setup and results

To validate the experimental setup, an experiment was carried out with the base fluid, where data were taken between the Reynold numbers of 1000 and 6000. Experimental data on the Nusselt number were compared with verified correlations, as available in the literature by Cengel and Ghajar [65]. Experimental results of the Nusselt number along the turbulent region are compared with the correlations of Dittus – Boelter and Notter and Rouse [65], as shown in Figure 6a.

Notter and Rouse's correlation correlates very well with the experimental data. It under-predicts the experimental data in the turbulent region within a maximum of 8% deviation. While in the laminar regime correlation of Morcos and Bergles, Depew and August were used to compare the experimental data. It is important to note that these two correlations were developed for the laminar mixed convection heat transfer condition, and they were found to correlate very well with the experimental data. Depew and August's correlation has shown a maximum deviation of 9.4%. Morcos and Bergle correlations correlate with experimental data within a maximum percentage deviation of 11%, with most of the data under 10% deviations, as shown in Figure 6b. On average, Morcos' and Bergles' correlations deviate from the experimental data by 5.8%, while Depew and August are within 2.27% on
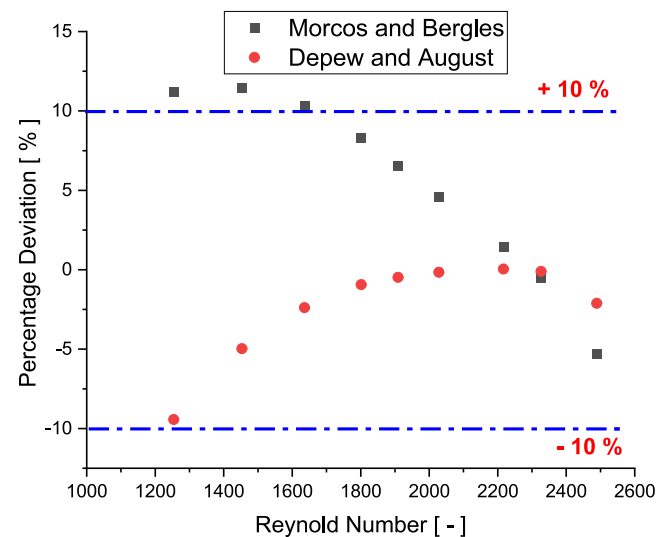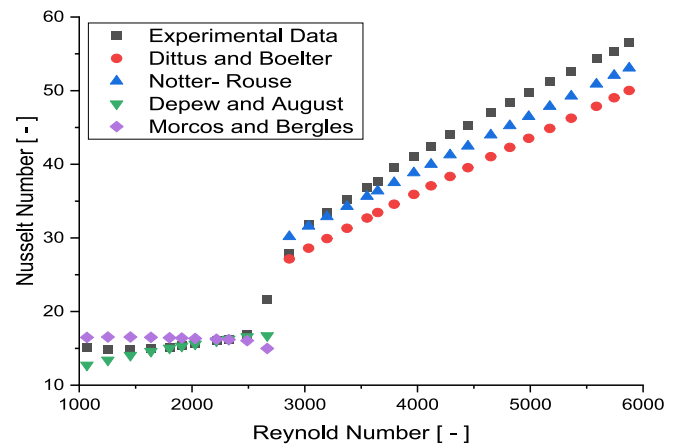

Figure 6. a) Experimental data (water) compared to the correlations b) percentage deviation of the experimental data with correlations in the laminar region.

average. These findings imply that the experimental setup operates reasonably well, and the conditions conform to laminar mixed convection flow conditions.

Dittus – Boelter Correlation

$$Nu = 0.023 \text{Re}^{0.8} Pr^{0.4} \qquad (31)$$

Depew and August Correlation

$$Nu = A \left(\frac{\mu_b}{\mu_w} \right)^{0.14} \left[Gz + C \left(GzGr^{\frac{1}{3}} Pr^{0.36} \right)^{0.88} \right]^{\frac{1}{3}} \qquad (32)$$

Where A = 1.75 or 2.11 depending on the and C = 0.12

Morcos and Bergles correlations

$$Nu = \sqrt{ \left[(4.36)^2 + \left[0.145 \left(\frac{Gr*Pr}{pw_f^{0.25}} \right)^{0.265} \right]^2 \right] } \qquad (33)$$

Where.

$Gr* = GrNu$ Defined as Modified Grashof number, while Pw_f is given as.

$$Pw_f = \frac{hd}{k_w t}$$

Notter and Rouse's correlation

$$Nu = 0.015 \text{Re}^{0.856} Pr^{0.347} \qquad (34)$$

3.6. Uncertainty analysis

Uncertainties of this experiments were estimated using a similar method used by Osman et al. [17] and Everts et al. [50], and this method was adopted from the work of Dunn et al. [66]. The uncertainties of experimental data for Nusselt number (Nu), coefficient of heat transfer (h), and Reynold number (Re), were obtained using the equations (35) – (37).

$$\delta Nu = \left[\left(\frac{\delta Nu}{\delta h} \delta h \right)^2 + \left(\frac{\delta Nu}{\delta D} \delta D \right)^2 + \left(\frac{\delta Nu}{\delta k} \delta k \right)^2 \right]^{1/2} \qquad (35)$$

$$\delta h = \left[\left(\frac{\delta h}{\delta \dot{q}} \delta \dot{q} \right)^2 + \left(\frac{\delta h}{\delta T_S} \delta T_S \right)^2 + \left(\frac{\delta h}{\delta T_b} \delta T_b \right)^2 \right]^{1/2} \qquad (36)$$

$$\delta \text{Re} = \left[\left(\frac{\delta \text{Re}}{\delta \dot{m}} \delta \dot{m} \right)^2 + \left(\frac{\delta \text{Re}}{\delta D} \delta D \right)^2 + \left(\frac{\delta \text{Re}}{\delta A_c} \delta A_c \right)^2 \right]^{1/2} \qquad (37)$$

Nusselt number (Nu), coefficient of heat transfer (h), and Reynold number (Re) uncertainties were found to be 3.3%, 6.6% and 5% respectively. Table 4 provides the list of the measuring instruments used in this experiments and their Uncertainties.

4. Results and Discussion

4.1. Laminar regime

Figure 7 shows that in the laminar regime, Al_2O_3 (60%) – MWCNT (40%) hybrid nanofluid has a much better-improved heat transfer characteristic than the other two hybrid nanofluids. When compared to Al_2O_3 (50%) – MWCNT (50%) nanofluid at Reynold number 1000, Al_2O_3 (60%) – MWCNT (40%) nanofluid has an enhancement of about 5.37%. Moreover, it is better than Al_2O_3 (40%) – MWCNT (60%) nanofluid with 5.20%. This shows that Al_2O_3 (50%) – MWCNT (50%) nanofluid has a slightly lower heat transfer capability in terms of Nusselt number compared to the other two fluids. Data analysis shows that its Nusselt number was slightly lower than that of Al_2O_3 (40%) – MWCNT (60%) by 0.172%, at Reynold number (Re = 1000). Heat transfer enhancement appeared to increase with the increase in Reynold's number. At Reynold number of approximately 1600, Al_2O_3 (60%) – MWCNT (40%) Nusselt number was found to be better than that of Al_2O_3 (50%) – MWCNT (50%) and Al_2O_3 (40%) – MWCNT (60%) with 6.58% and 6.2% respectively. However, Nusselt number of Al_2O_3 (50%) – MWCNT (50%) further deteriorated when compared to the Al_2O_3 (40%) – MWCNT (60%) nanofluid. Because it is lower than that of Al_2O_3 (40%) – MWCNT (60%), by about 0.4 %, as against 0.172% at Re = 1000.
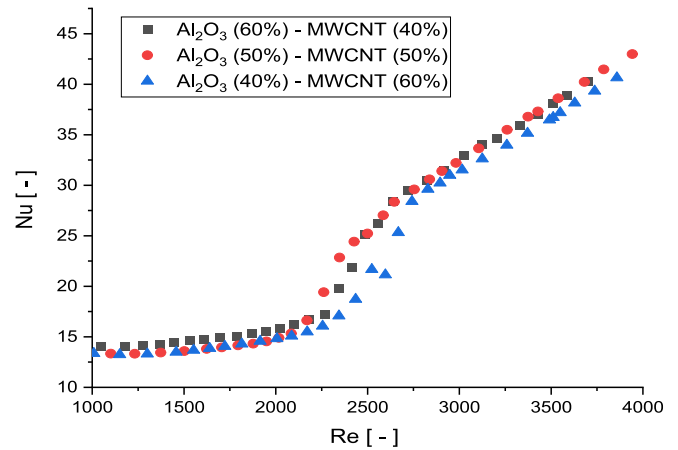
Figure 7. Nusselt number as a function of Reynold number for the three hybrid nanofluids

Table 4
Measuring instruments and their uncertainties

Measuring instruments	Make / Type	Specifications/ Range	Accuracy/ uncertainty
Thermocouples	T – Type Thermocouples	-250°C to 400°C	0.1 °C.
Flow meters(Coriolis flow meter)	CmFs015	0.204kg/min - 4.09kg/min	0.1 %
Pressure Transducers	Omega 10WDWUI	0 - 17 Kpa	0.25%
Power SupplyVoltageCurrent	KIKUSUI PWR800M	- 320V 0 - 12.5 A	V 0.04 A
Thermal Conductivity	KD2 Pro Thermal conductivity meter	Controller: 0 to 50°CSensor; - 50 to +150°C	5% from 0.2 to 2 W/mK and0.01 from 0.02 to 0.2 W/mK
Viscosity	Sv–10 Vibro Viscometer (A&D, Japan),	Range; 0.3 - 10,000 mPa・sOperating Temperature: 10 - 40°C	Less than 1% at Full scale
Ph Meter	H198129 / H198130 Waterproof pH COMBO. Henna Instruments	0 - 4000 $\mu s/cm$	0.05
Electrical conductivity	CON 700 conductivity meter	0 μS to 200.0mS	1 %

4.2. Transition and turbulent regime

In transition and turbulent regimes, analysis shows that Al_2O_3 (40%) – MWCNT (60%) nanofluid Nusselt number deteriorates as compared to the other two fluids in consideration. At a turbulent Reynold number of 3700 and 3000, Al_2O_3 (50%) – MWCNT (50%) nanofluid was better than Al_2O_3 (40%) – MWCNT (60%) by 2.23% and 2.15%, respectively. While Al_2O_3 (60%) – MWCNT (40%) is better than Al_2O_3 (50%) – MWCNT (50%) nanofluid, with a very slight margin of about 0.0599 and 2.21% respectively. Al_2O_3 (60%) – MWCNT (40%) also performs better than Al_2O_3 (40%) – MWCNT (60%) with 2.28 and 4.32% at the same Reynold numbers.

Nevertheless, in the transition regime, Al_2O_3 (50%) – MWCNT (50%) nanofluid performance was better. At Reynold numbers 2400 and 2550, its Nusselt number values are better than Al_2O_3 (60%) – MWCNT (40%) values with 11.7% and 3.0%, respectively. When compared with Al_2O_3 (40%) – MWCNT (60%) nanofluid, Al_2O_3 (50%) – MWCNT (50%) is better with 23.36% and 21.79% at the same Reynold numbers. This shows that at the transitional flow regime, the enhancement in Nusselt number is better with the Al_2O_3 (50%) – MWCNT (50%) nanofluid. while in the turbulent and laminar regime, Al_2O_3 (60%) – MWCNT

(40%) has the better heat transfer characteristics.

These results portrayed the PWC's significant influence on this hybrid nanofluid's convective heat transfer characteristics. It also shows that having different PWC makes the fluid entirely different despite having the same nanoparticles and volume concentrations.

4.3. Influence of the axial position on force convection heat transfer

4.3.1. Effect on the temperature profile

Heat transfer characteristics at different axial positions normally change from one axial position to another. Several factors are believed to be responsible for these variations. The most obvious ones are the thermal entrance effects and the temperature difference. Temperature differences may be due to the temperature gradient along the tube length or due to the radial temperature difference. This temperature difference is very important concerning the force convection heat transfer, especially with nanofluid. Because nanofluid viscosity is significantly affected by temperature. Ghajar and Tam [67] explained that the effects of radial temperature mainly result in free convection heat transfer.

An increase in temperature along the tube length results in the radial
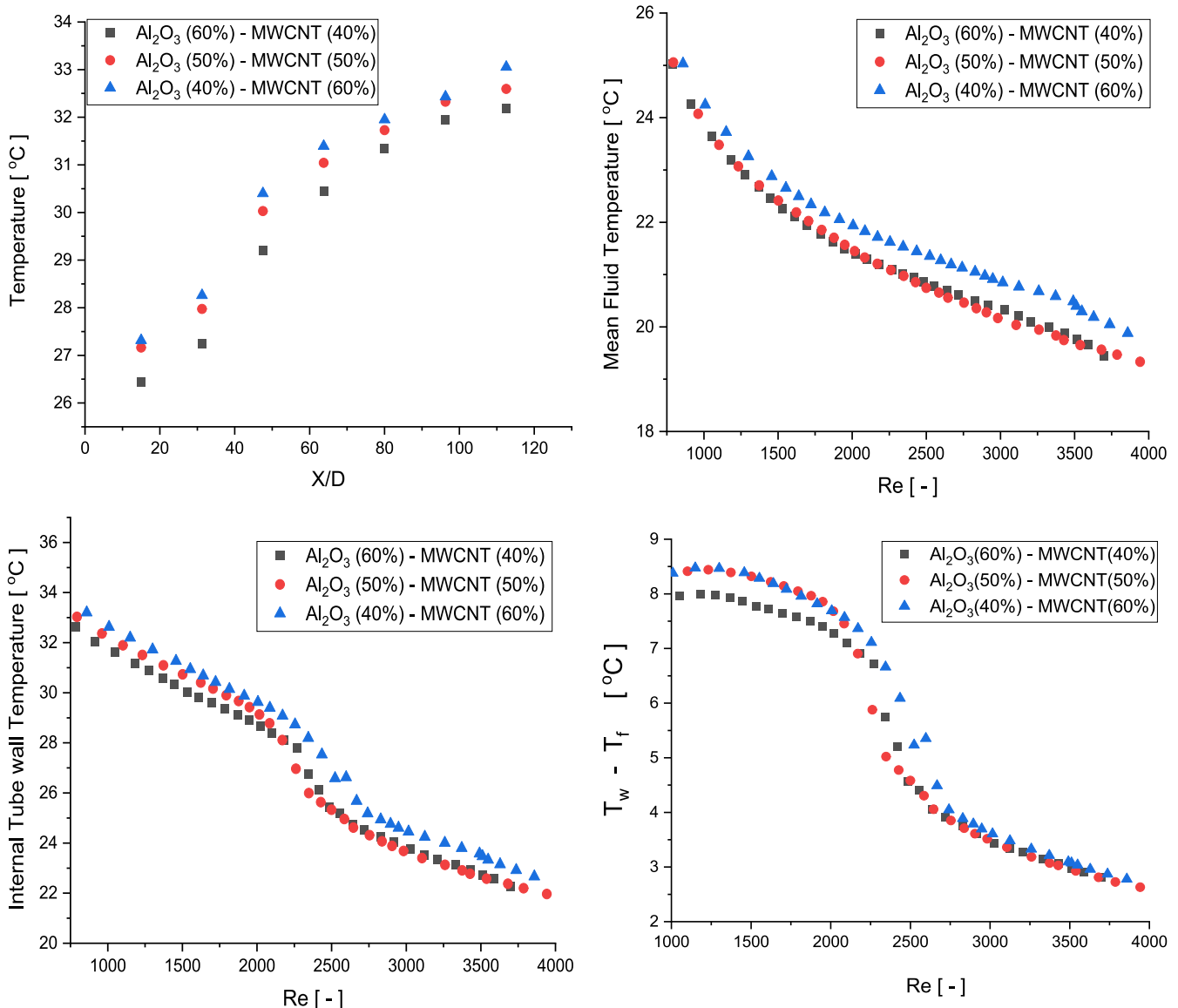

Figure 8. Temperature Profile Graphs for the Three Hybrid Nanofluids

temperature increase across the tube length (i.e., with the increase of the distance from the tube inlet X/D). Figure 8a shows the tube internal wall temperature (T_w) as a function of the axial positions (X/D) at a Reynold number 1600. As the axial distance (X/D) increased, internal tube wall temperature also increased. This signifies that the fluid density and viscosity will decrease across the tube length. Experimental data from the literature and this study also confirmed that nanofluid viscosity decreases with an increase in temperature Figure 2. Figure 8d shows the

radial temperature profile of the three fluids as a function of Reynold number. Results show that the fluid's radial temperatures decrease with increasing Reynold number, and its peak value is at the laminar region. This shows the effects of Reynold's number on the radial temperature. Therefore, it's obvious that the radial temperature increases with the x/d from the tube inlets and decreases as the Reynold number increases. This is very significant because it will help understand radial temperature's influence on mixed convection. Ghajar and Tam [67] stress that
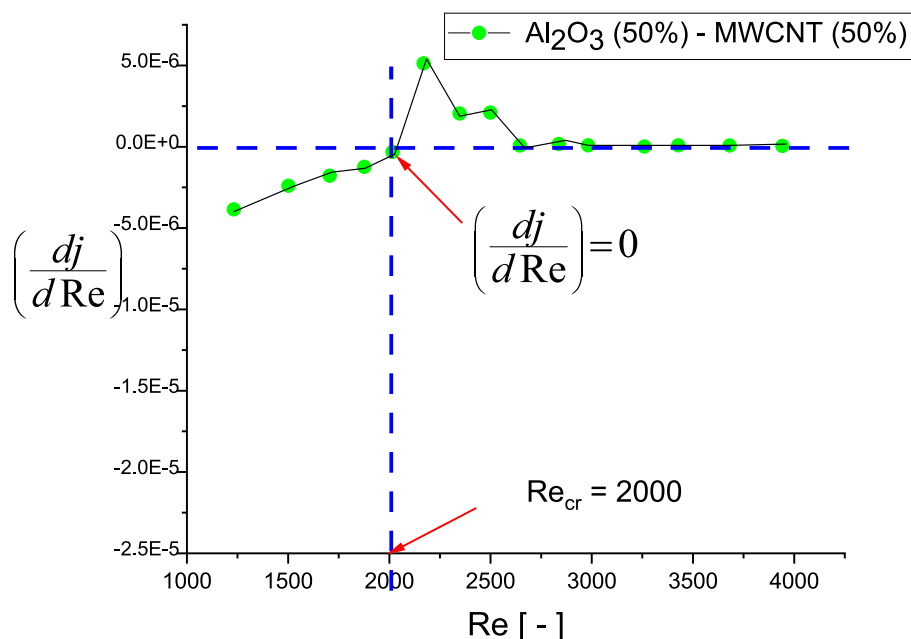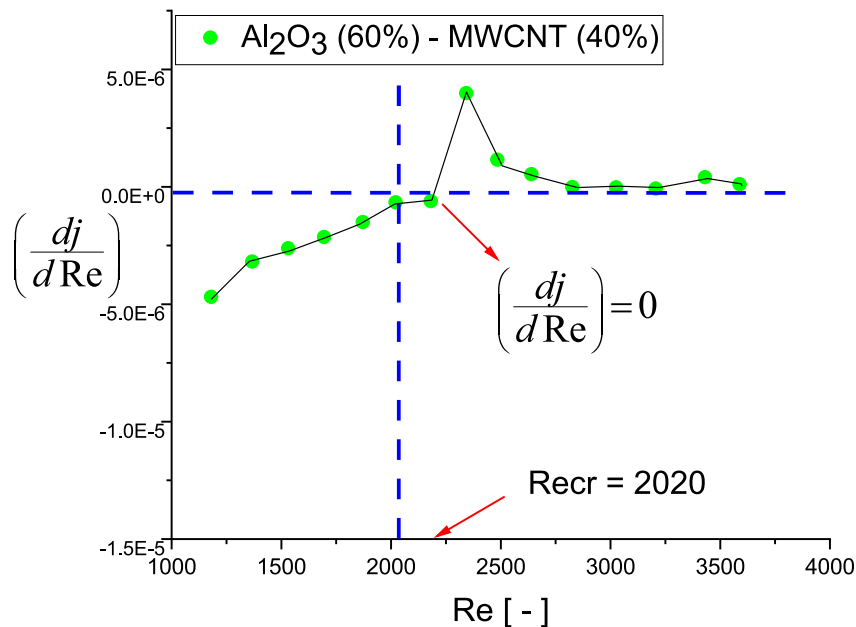

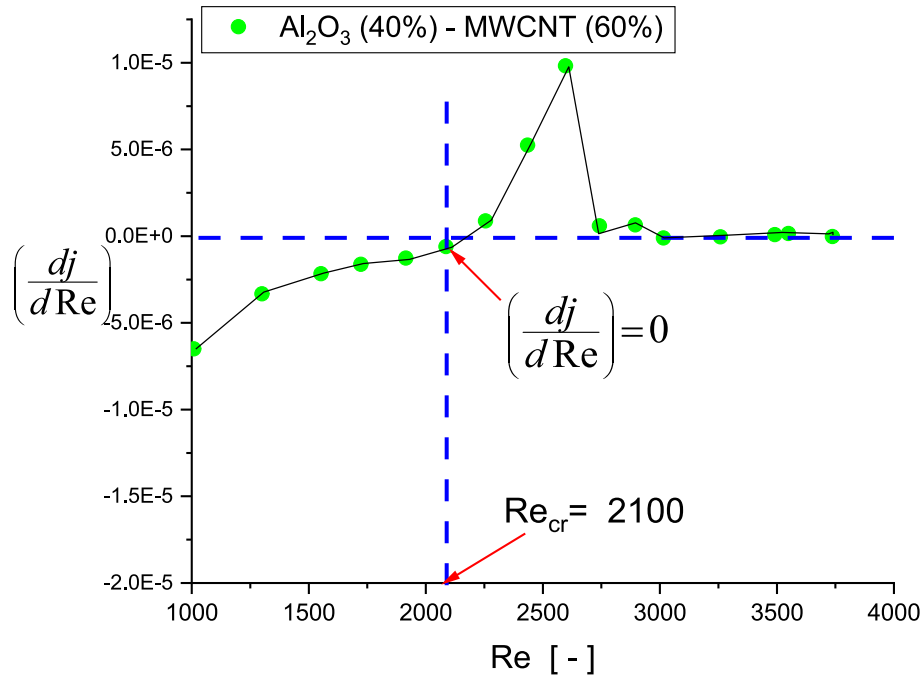**Figure 9.** Critical Reynold number

Figure 9. (*continued*).

radial temperature is very significant with regard to the development of mixed convection.

From Figure 8, it was also noticed that during force convection heat transfer, both the fluid main temperature (T_f) and internal fluid wall temperatures decrease with the increase in Reynold number (i.e., as shown in Figure 8(b-c)). This reaffirmed that fluid properties, especially viscosity and density, will vary with the increase in Reynold's number. It is also essential to note that not only viscosity and density are temperature dependent, but thermal conductivity is also temperature dependent. Variation of these temperature-dependent properties significantly affects the fluid heat transfer characteristics.

4.4. Effects of PWC on critical Reynolds number

Initially, it was widely believed that the critical Reynold number or transition start at a Re = 2300. However, experimental research works by Meyer and Oliver [68], Nagendra et al. [69], and Ghajar and Tam [70] proved otherwise, as their results show that the critical number is dependent on several factors. This includes the tube inlet configuration type, fluid properties, heat flux, etc. Osman et al. [17]. Research findings show that nanofluid viscosity was why the transition started earlier with nanofluid than with base fluid (water). In this research work, the critical Reynold numbers for the three fluids were identified using the method suggested by Everts et al. [71] and Andrade et al. [72], as presented in equation (38). Using this method, a critical Reynold number (Re_{cr}) is defined as the Reynold number at which the Colburn j factor gradient changes from negative to positive, or simply as the Reynold's number at which gradient of Colburn J factor is equal to zero as shown in Figure 9.

Re = Re_{cr}, When

$$Re = \left(\frac{dj}{dRe}\right) = 0 \qquad (38)$$

The critical Reynold numbers for the three hybrid nanofluids were found to differ slightly. For Al$_2$O$_3$ (60%) – MWCNT (40%), the start of the transition is 2020, and for Al$_2$O$_3$ (50%) – MWCNT (50%), the critical Reynold number is 2000, while for Al$_2$O$_3$ (40%) – MWCNT (60%) started at critical Reynold number of 2100. Figure 9 shows the graphical representation of equation (38).

This finding shows that the PWC of hybrid nanofluids affects the force convective flow characteristics of these fluids. It's obvious that force convective heat transfer of hybrid nanofluids also depends on the PWC.

4.5. Laminar forced–mixed convection heat transfer of hybrid nanofluid.

4.5.1. Thermal entrance effects

Figure 10 shows the local Nusselt number at different axial positions as a function of the Reynold number. From the plot, it was noticed that from the axial position x/d = 15 to x/d = 112.5, there is variation in the Nu(x) with the Reynold number, which is obvious with all three hybrid nanofluids. This variation in Nu(x) with the axial position may be associated with free convection effects and thermal entrance effects. Free convection effects occur due to high radial temperature (i.e., Figure 8d), which results in the formation of buoyancy-induced secondary flow normally along the laminar region.

Considering Figure 10, at X/D = 15 and X/D = 31.25, local Nusselt numbers increase as the Reynold number increases. And Nusselt numbers at X/D = 15 and X/D = 31.25 are much higher than those at the other axial position. In contrast, from the axial position X/D = 47.5, the trend of the Nusselt number changes. It starts to decrease with an increase in Reynold's number. Its values (Nusselt number) are lower compared to the first two axial positions (i.e., X/D = 15 and X/D = 31.25). The reason for the higher local Nusselt number at the first two axial positions is due to the thermal entrance effects. By carefully considering position x/d = 15 and x/d = 31.25, the Nusselt number is increasing with the increase of Reynold number. This signifies that the thermal boundary layer at that position is very thin (i.e., thermally developing region), and the flow can be regarded as thermally developing flow. Shome et al. [27] explained that at an axial position close to the tube inlet, the heat transfer increased due to the entrance effects and variable viscosity. Therefore, the enhancement in the Nusselt number at those two axial positions (x/d = 15 and x/d =31.25) are not due to the mixed convection but rather due to the entrance effects. However, the possibility of the free convection effect cannot be ruled out entirely for now. But, it is certainly not the dominant, as the thermal entrance effects are expected to be very significant at those two positions. There are
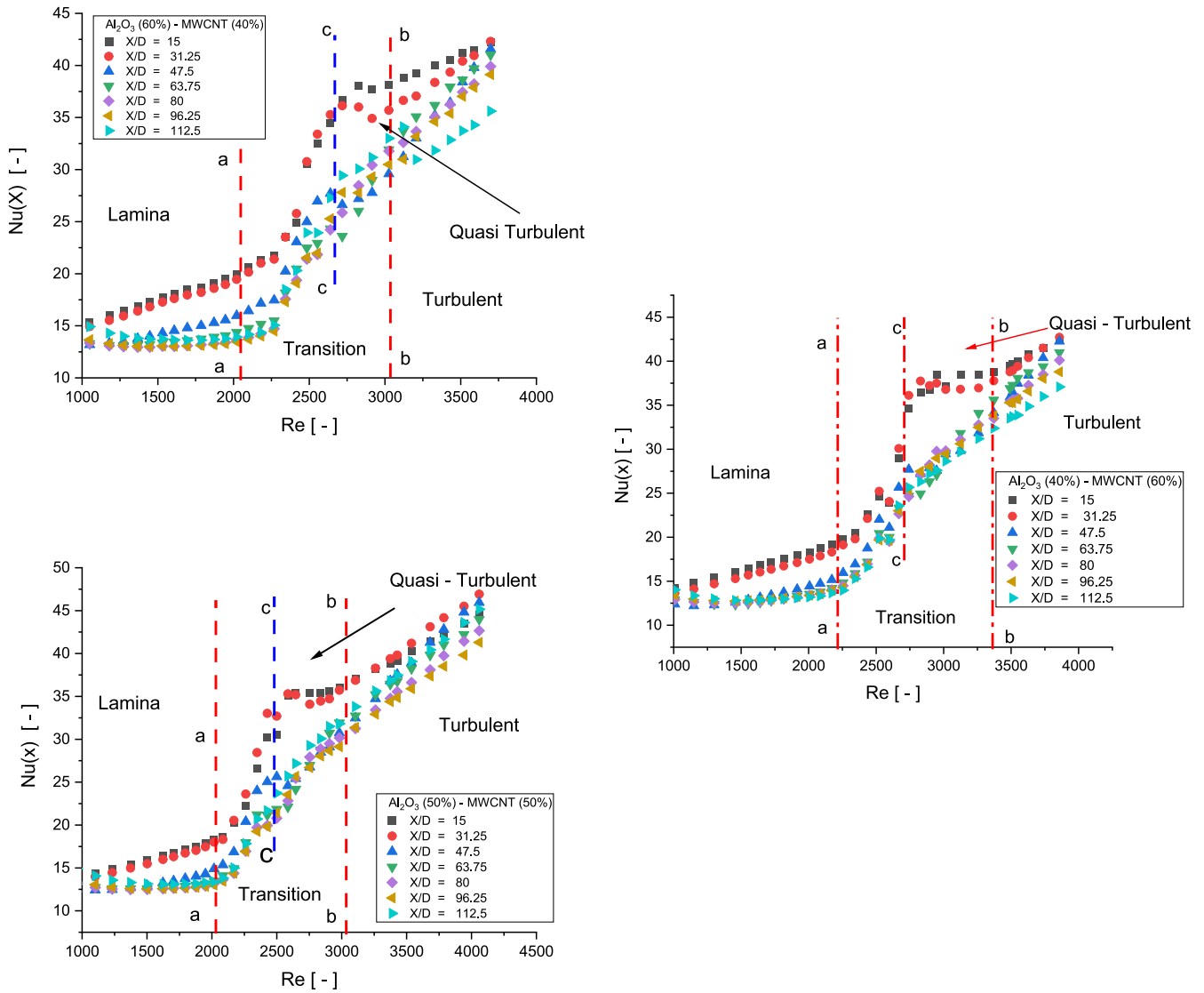
Figure 10. Variation of Local Nusselt number at different axial positions as a function of Reynold number.

many criteria for differentiating the mixed convection boundary regions and other regions of the flow. Ghajar and Tam [51] and Everts et al. [71] have suggested different methods by which we can quantitatively and objectively characterise these regions. In this research, the method suggested by Everts et al. [71] was employed.

According to Everts et al. [71], we can differentiate these two regions from each other by using equations (39) and (40). According to equation (39), the thermal entrance effect is dominant if the gradient of the Nusselt number with respect to the Reynold number is greater than zero. Mathematically;

$$\frac{dNu}{dRe} > 0 \qquad (39)$$

Meanwhile, mixed convection effects are the most dominant if the gradient is less than zero. This can also be expressed mathematically as given in equation (40).

$$\frac{dNu}{dRe} < 0 \qquad (40)$$

Therefore, in these experiments, we used these two equations, adopted from Everts et al. [71], to differentiate the regions around the tube where mixed convection effects are most dominant.

Figure 11 presents the plots of the gradient of the local Nusselt number against the Reynold number at an axial position of X/D =15 for the three hybrid nanofluids. The plots show that the gradient is greater than zero along the laminar Reynold numbers for the three hybrid nanofluids. This shows that, at this axial position, the entrance effect is the most dominant and is responsible for the increase in the local Nusselt number at those two positions. This also signifies that the thermal boundary layer is still developing [71]. Subsequently, the flow can be categorized as a thermally developing flow. Since the thermal boundary layer is still developing.

Figure 12 presents the plots of the gradient of the local Nusselt number against the Reynold number for the two axial positions of x/d = 63.75 and 96.25. It is important to note that, in this analysis, our consideration is only on the laminar regimes, and in this regard, Reynold's number between 1000 and 2400 is our primary consideration. Equation (40) shows that mixed convection influence becomes more significant at an axial X/D = 63.75 and X/D = 96.25. Because equation (40) becomes less than zero. This can be seen with all three hybrid nanofluids. The condition in equation (40) was satisfied. This also indicates that thermal boundary layer thickness developed significantly at those axial positions. Yunus and Cengal [65] explained that thermal boundary layer thickness increases across the tube length (i.e., its thickness increases as the X/D distance from the tube inlet increases). In
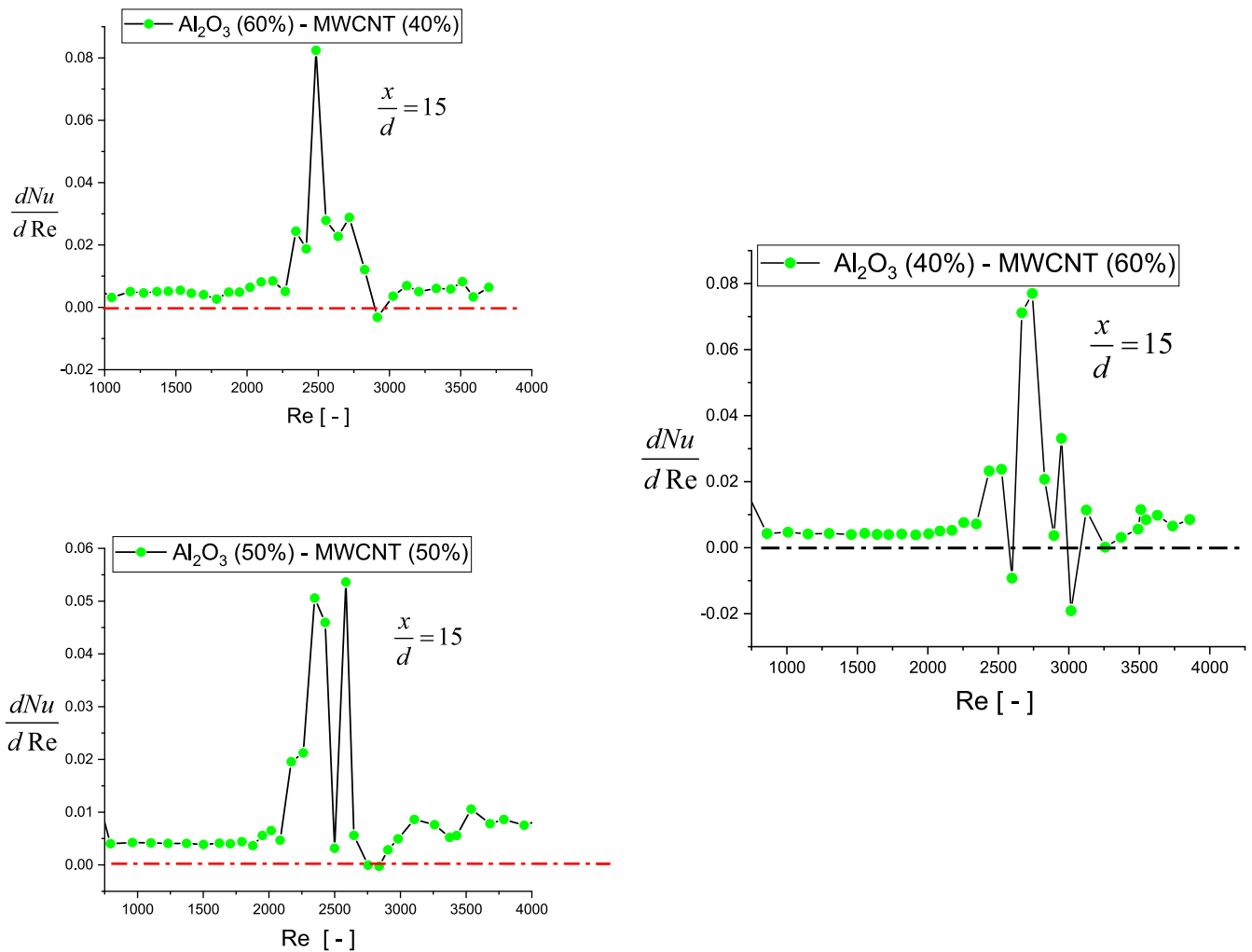
Figure 11. Gradient of Nusselt Number as A Function Reynold Number at X/D = 15 Axial Position

contrast, the thermal entrance length decreases as the thickness develops [71]. Therefore, free or buoyance-induced secondary flow starts to dominate, and this is because of the rise in radial temperature and wall temperature across the tube length, as shown in Figure 8.

Figure 12 shows that mixed convection influences for Al_2O_3 (60%) – MWCNT (40%) hybrid nanofluid are only significant between the Reynold number of 1000 to 1400. While with the Al_2O_3 (50%) – MWCNT (50%) and Al_2O_3 (40%) – MWCNT (60%) hybrid nanofluid is significant between the Reynold number range of 1000 – 1380. This shows that with regard to the range where the mixed convection influence is significantly more substantial, the difference between the three fluids is minimal.

4.5.2. Evaluation of the mixed convection significance

In Figure 13, experimental data is compared with the Ω_F given in equation (30). As explained earlier, the higher the experimental data deviate from the Ω_F the more significant the influence of mixed convection. Two axial positions were considered in this regard (X/D = 63.75 and 96.25) since it was already established in section 7.5.1 that at x/d = 15, the entrance effect is the most dominant and responsible for the increase in heat transfer. It can be seen that, at an approximate Reynold number of 1000 and x/d = 63.75, experimental data deviate from equation (30) by a maximum of about 41.0%, with Al_2O_3 (60%) – MWCNT (40%). Which is the highest. This shows that the mixed convection effects showed better strength with the Al_2O_3 (60%) – MWCNT (40%) than with the other two fluids in the laminar region.

However, the difference between them is not very significant. While at an axial position of X/D = 96.25, mixed convection strength tends to reduce significantly compared to the other axial position (i.e., X/D =63.75).

Figure 13 shows Ω compared to equation (30) as a function of Reynold number at the axial position of X/D = 96.25. Results show that all three fluids (Al_2O_3 (60%) – MWCNT (40%), Al_2O_3 (50%) – MWCNT (50%) and Al_2O_3 (40%) – MWCNT (60%)) deviate from the equation Ω_F by almost the same percentage. Even more closed than what is experienced in the previous position x/d = 63.75. This shows that varying their percentage weight compositions has not shown much difference in their mixed convection behaviour. As the fluids were barely different from each other in terms of the mixed convection characteristics. It is also noticed that the significance of the mixed convection decreases as the X/D distance from the inlet increases. Because, at X/D = 96.25 and Reynold number of 1000, Ω only deviate from the Ω_F by about 14.7% with Al_2O_3 (60%) – MWCNT (40%). However, at X/D = 63.75, the deviation was 41.0%. This is because, at the axial position X/D = 63.75, the thermal boundary layer is still developing, so there is still an influence of the entrance effects, and together with the developing secondary flow influence, Ω was enhanced even further, Meyer et al. [66] described such conditions as mixed convection developing region.

When the laminar Reynold number increases from 1000 to around 2100, we notice that mixed convection significance decreases for both axial positions (X/D = 63.75 and 96.25) as the Reynold number increases. At the Reynold number of 2100 and x/d = 63.75, Al_2O_3 (60%) –

MWCNT (40%) deviate from the equation Ω_{F_r} by about 32.3% while Al$_2$O$_3$ (50%) – MWCNT (50%) and Al$_2$O$_3$ (40%) – MWCNT (60%), with 29.2% and 27.93% respectively.

While at the same Reynold number but at an axial position of X/D = 96.25, the deviation from equation (30) reduced significantly compared to the previous position. Al$_2$O$_3$ (60%) – MWCNT (40%) only deviated with about 9.29%, while Al$_2$O$_3$ (50%) – MWCNT (50%) and Al$_2$O$_3$ (40%) – MWCNT (60%) deviated with 8.66% and 9.07%. At a low Reynold number of approximately 1000, mixed convection influence appeared to have reduced as the X/D distance from the inlet increased. Percentage deviation by the three fluids reduced to 14.7 %, 12.79 %, and 14.48%, respectively. Feng et al. [29] and Li et al. [23] reported similar results where the mixed convection influence of SiO$_2$ nanofluid reduced significantly with the increase in Reynold number, which agrees with our finding. The reason behind the reduction in the mixed convection influence, as the Reynold increases, is that both the radial temperature and fluid mean temperature decrease as the Reynold number increases (Figure 8). This reduction in fluid and radial temperature results in an increase in fluid viscosity and density. High fluid density and viscosity restricted dispersed nanoparticle motion, and low wall temperature limit suppressed the formation of the buoyance-induced secondary flow. These conditions suffocated the natural convection influence and subsequently reduced its impact.

To better understand the Reynold number effect on the mixed convection. Figure 14 shows another dimensionless parameter called Raleigh number (Ra). Ra number also signifies the strength of the mixed convection. From figure 14, Ra also decreases as the Reynold number increases. Ra number magnitudes are much higher in the laminar region than in the transition and turbulent regions. However, it is interesting to know that axial position has very little or no influence on its magnitudes (Ra) as presented. (i.e., Figure 14).

4.6. Mixed convection in transition and turbulent regions

To analyse our experimental data in the transition and turbulent region, we are going to consider Figure 8, Figure 10, Figure 14, and Figure 15. Due to the nature of the transition regime, Figure 13 cannot be used to analyse the results. Because there are no satisfactory pure force convection correlations that are valid within the transition regime, especially with the nanofluids. Thus, it would be better to analyse the results based on the Richardson number and Raleigh number.

It is well known that transition and turbulent regimes are characterised by high fluctuations due to high flow rates as compared to lamina regimes. From Figure 8, we noticed that an increase in Reynold's number resulted in a temperature decrease, which is true with all temperature profiles. (i.e., internal tube wall temperature, radial
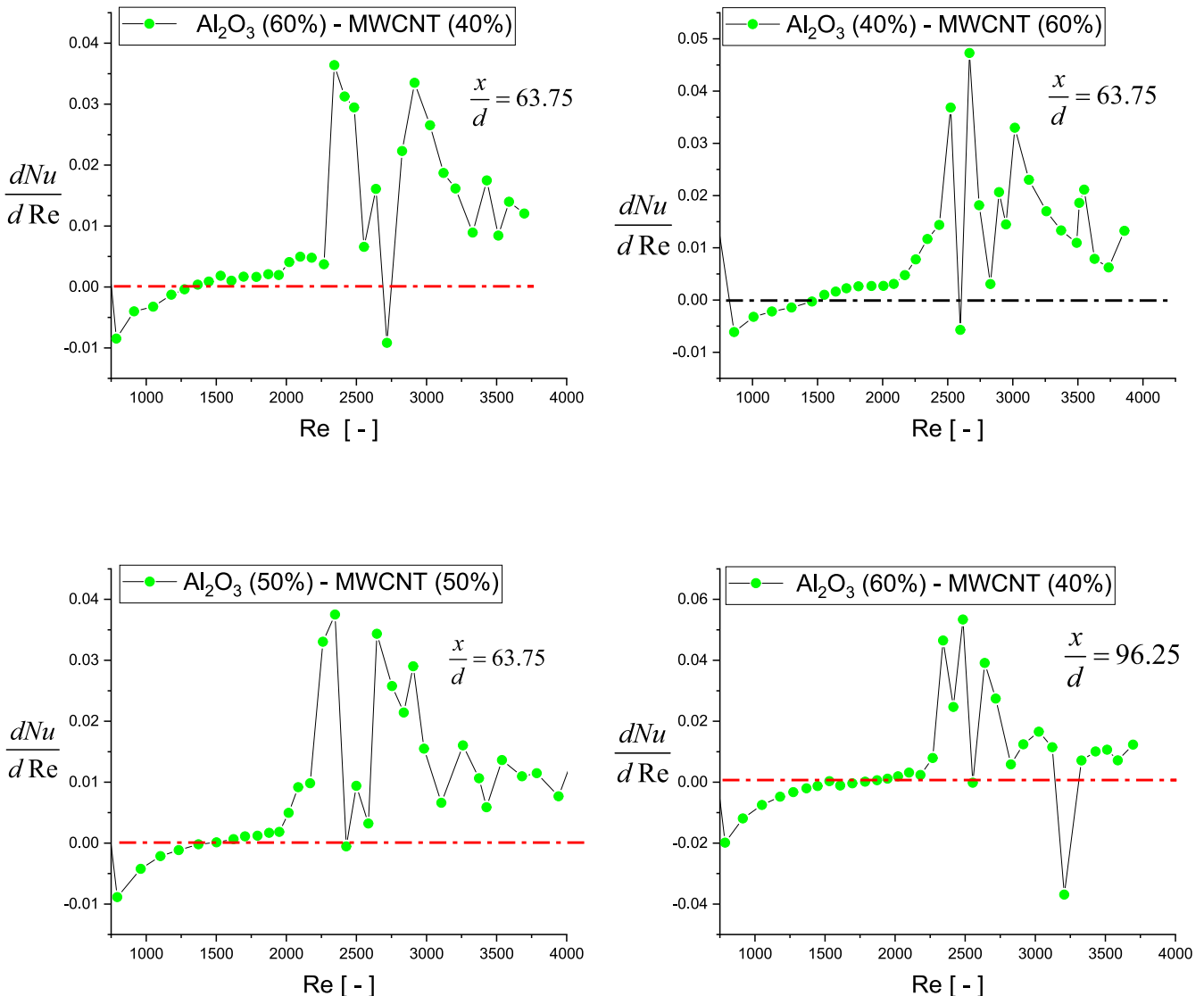

Figure 12. The gradient of Nusselt number as a function Reynold number at X/D = 63.75 and 96.25 axial Positions

$$\frac{dNu}{d\,Re}$$

Al$_2$O$_3$ (50%) - MWCNT (50%)

$$\frac{x}{d} = 96.25$$

Re [-]

$$\frac{dNu}{d\,Re}$$

Al$_2$O$_3$ (40%) - MWCNT (60%)

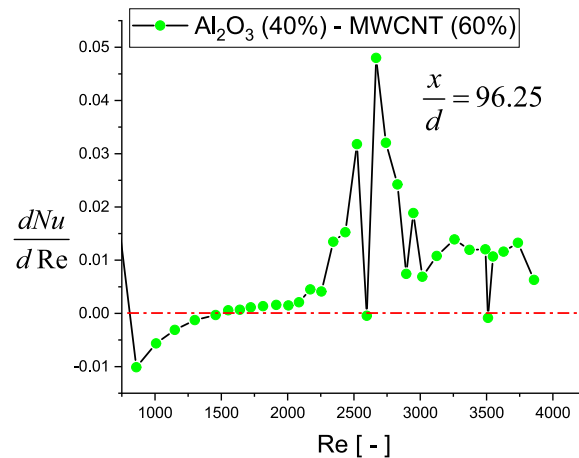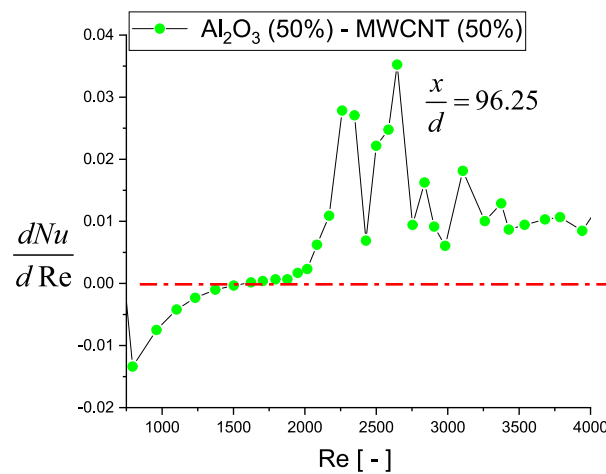$$\frac{x}{d} = 96.25$$

Re [-]

Figure 12. (*continued*).

temperature, and mean fluid temperature). This significantly impacts the development of free convection because as the temperature decreases, the fluid viscosity increases. The increase in fluid viscosity will suppress the secondary induced buoyance force (i.e., free convection effects). As such, the impact of the free convection within transition and turbulent flow is not very significant. By considering Figure 14 which shows the influence of the Reynold number on the Raleigh number at two axial positions (i.e., X/D = 63.75 and 96.25). Results show how Ra number decreases as the Reynold number increases. This decrease in the Ra signifies the reduction of the free convection influence.

Figure 15 presents a graph of the Richardson number against the Reynold number. As explained by Cengal et al. [65] and Evert et al. [73], the Richardson number is a dimensionless parameter which represents the ratio of buoyant forces (i.e., secondary flow) to the viscous force. It is a parameter that quantifies the strength of free convection. When the Richardson number is below 0.1, the flow is expected to be dominated by forced convection. In contrast, if the Richardson number is above 10, it was expected that the flow was purely dominated by free convection. However, when the Richardson number fluctuates between 0.1 and 10, the flow is anticipated to be in the mixed convection flow regime.

From Figure 15, it can be seen that all the lamina data were within the mixed convection region, which agreed with our earlier analysis with parameter Ω. From the result shown in Figure 15 and according to

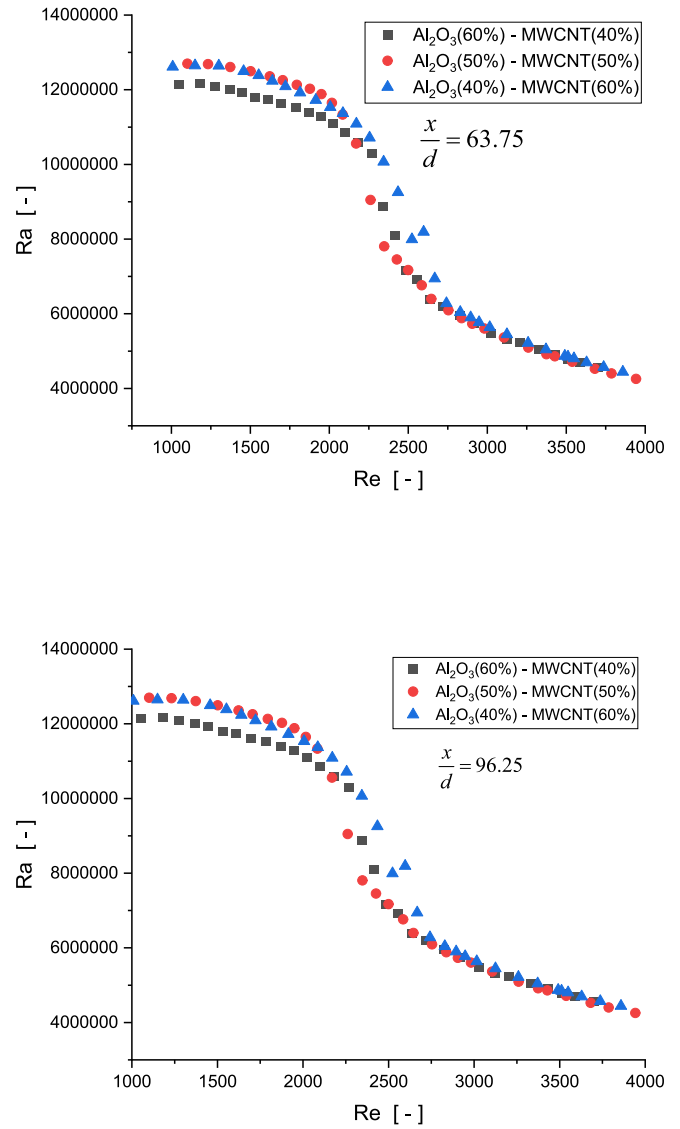the interpretation of Evert et al. [71], mixed convection exist in the transition region at both the two axial positions x/d =63.75 and 96.25. Because Ri number values fall within the range of 0.1 – 0.4, which shows a mixed convection condition exists. While, in a turbulent region, there is no sign of mixed convection, more especially from the Reynold number above 3000. Because Ri's number was below 0.1. This shows that force convection was dominant in the turbulent region. Similar to the Ra number, the Richardson number was also found to be independent of the axial position. The absence of free convection in the turbulent region is not surprising because of the influence of the fluid viscosity and density, which increase with the decrease in temperature. Manay et al. [40] explained that the slip mechanism in nanofluid convective transports differs and is highly inconsistent, but the most significant ones are due to the thermophoresis and Brownian motion. Considering these two important parameters, Figure 8 explains why free convection effects decrease with the increase in the Reynold number. The most obvious reason is that they are temperature-dependent. Therefore, a decrease in temperature not only affects the fluid viscosity but also results in the reduction of Brownian motion and thermophoresis, and as such, results in the decrease or suppression of the free convection effects.
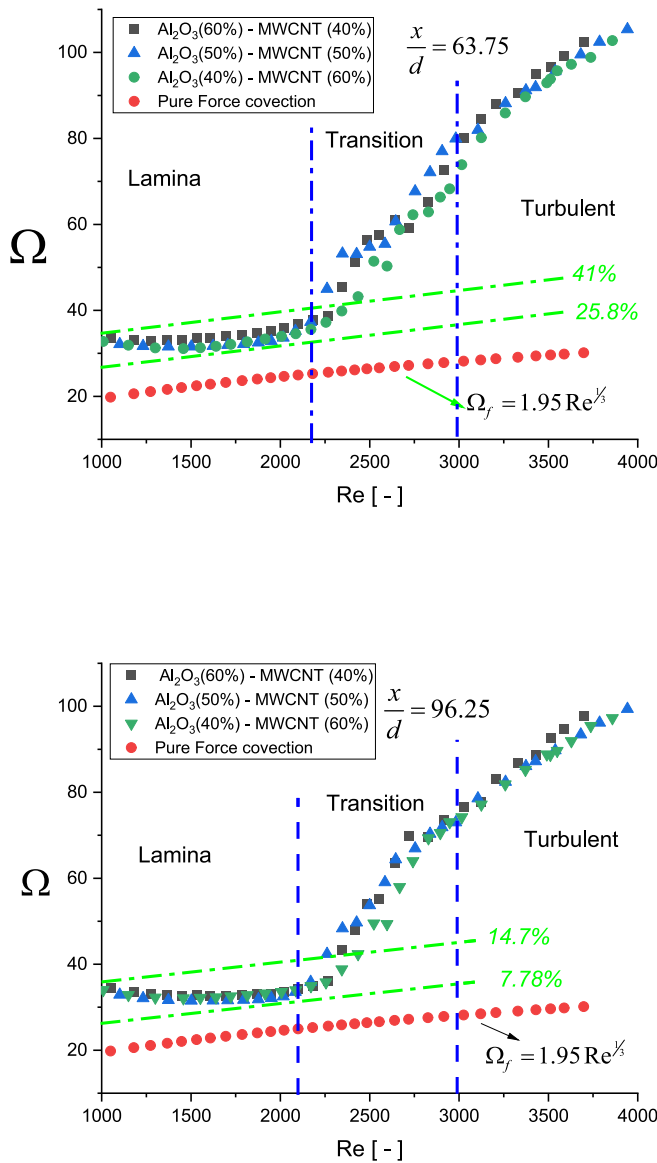
Figure 13. Graphs of Parameter Ω Compared to Ω_F as a function of Reynold number at Axial position X/D = 63.75 and 92.25

Figure 14. Graphs of Raleigh number as a function of Reynold number at Axial position X/D =63.75 and 92.25.

4.7. Thermal entrance effects on the transition and turbulent region

From Figure 10, we already established that the entrance effect was dominant at the axial position X/D = 15 and x/d = 31.25. The increase of the Nusselt number with Reynold is due to the developing thermal boundary thickness, which is very thin, which results in the laminar Nusselt number trend differing from the other axial positions. Subsequently, by considering the transition and turbulent region, we notice that along the two axial positions, x/d =15 and x/d = 31.25, the trends at the end of the transition differ from the rest of the axial positions. There is a fluctuation of the Nusselt number just before the turbulent region (i.e., between the line cc and bb), and this was seen with all three fluids. Everts et al. [71] explained that, just before the turbulent region, there is another regime called the quasi-turbulent regime. This is another distinctive flow regime with characteristics that differ from the transition and turbulent region. This regime is often regarded as part of the transition region. Because the flow was not fully turbulent at that point [71,74]. Detailed characteristics of this flow regime have not yet been investigated. However, Everts et al. [71] found that this flow regime is affected by axial positions. Its start and end, i.e., the Range of

the Quasi-turbulent, often varied as the X/D changes. Figure 10 shows that this flow regime (i.e., Quasi –Turbulent flow regime) exists only at the tube axial positions where thermal entrance effects are very significant. As the distance X/D from the tube inlet increases, its influence or its existence disappears. This shows that this flow regime is significant at positions where the thermal boundary layer thickness is very thin and tends to disappear as the flow develops into a fully thermally developed flow.

5. Conclusion

An investigation into force and mixed convection heat transfer characteristics of hybrid nanofluids is conducted with three hybrid nanofluids of Al_2O_3 – MWCNT (i.e., Al_2O_3 (60%) – MWCNT(40%), Al_2O_3 (50%) – MWCNT(50%) and Al_2O_3 (40%) – MWCNT(60%)). From the experimental results and analysis, conclusions were drawn and summarised as follows;

- Results show that percentage weight composition PWC significantly influences hybrid nanofluid heat transfer characteristics. In lamina region heat transfer was better enhance with Al_2O_3 (60%) – MWCNT
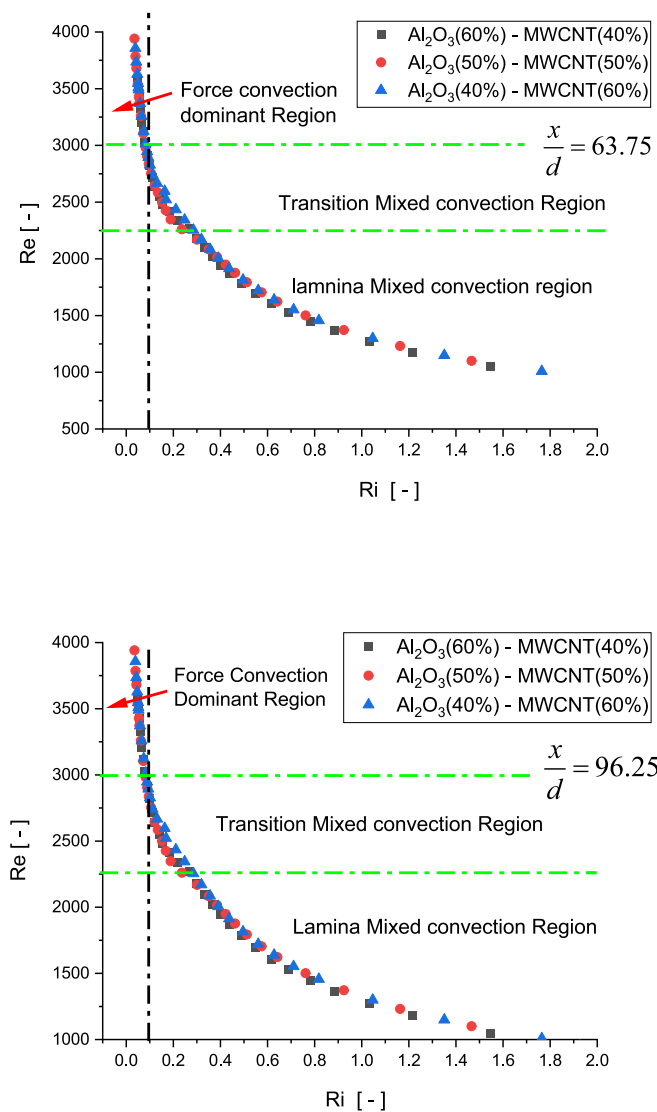
Figure 15. Reynold number as a function of Richardson Number at two axial positions of X/D = 63.75 and 92.25.

(40%), then followed by Al_2O_3 (40%) – MWCNT(60%) with 5.37% and 5.20% better than Al_2O_3 (50%) – MWCNT(50%). In the transition region, Al2O3 (50%) – MWCNT(50%), nanofluid has the best heat transfer enhancement, with an enhancement of about 11.7% at a Reynolds number of 2400.

- It was also found that varying the PWC of hybrid nanofluids also affects their transition boundaries. This was clearly shown as the critical Reynold number of the three hybrid nanofluids differs despite having the same volume concentration and particle sizes. Results show that transition starts at different critical Reynold numbers. The critical Reynold number of Al_2O_3 (40%) – MWCNT(60%) is 2100, while Al_2O_3 (60%) – MWCNT(40%) and Al_2O_3 (50%) – MWCNT (50%) are 2020, and 2000 respectively. Even though the PWC varied by only by 10%, its significance was shown in the fluid characteristics.
- Thermal entrance effects resulted in a much higher heat transfer enhancement than mixed convection effects. This was true for all the flow regimes (i.e., lamina, transition, and turbulent). It was also found that, unlike the mixed convection effects, entrance effects extend to all the flow regimes. Along the entrance region, the local Nusselt number increases with the increase in Reynold number.

- It was found that equations (39) and (40) correctly characterise and identify the boundaries between entrance region and mixed convection dominant region. It correctly distinguishes the entrance and region where mixed convection influence is the most dominant. These findings would help in analytical studies of hybrid nanofluids.
- Results show that mixed convection effects are more significant in the laminar region than in the transition and turbulent region. However, the impact of the mixed convection varied with both the axial position and Reynold number. Al_2O_3 (60%) – MWCNT (40%) have shown higher strength of the mixed convection than the other two hybrid nanofluid fluids with 'Ώ value of about 41%. It was also found that mixed convection effects decreased with the increase in axial position from tube inlet. Its value deteriorates from 41% at x/d = 63.75 to 14.7% at x/d = 96.25.

6. The future scope and limitation

This research findings were based on thermally developing flow conditions. Fully developed flow conditions were largely not considered in this research. Therefore, it is suggested that hybrid nanofluids forced – and mixed convection heat transfer characteristics to be investigated under fully developed flow conditions as well.

CRediT authorship contribution statement

Ibrahim Umar Ibrahim: Writing – original draft, Validation, Methodology, Investigation, Formal analysis, Data curation, Conceptualization. **Mohsen Sharifpur:** Writing – review & editing, Visualization, Validation, Supervision, Resources, Project administration, Methodology, Investigation, Funding acquisition, Conceptualization. **Josua P. Meyer:** Writing – review & editing, Supervision, Resources, Project administration, Funding acquisition.

Declaration of competing interest

The authors declare that they have no known competing financial interests or personal relationships that could have appeared to influence the work reported in this paper.

Data availability

Data will be made available on request.

References

[1] S. Nallusamy, M. Rajaram Narayanan, J. Logeshwaran, 'Synthesis and machining characterization of copper-multiwalled carbon nanotubes-graphene hybrid composite using SEM and ANOVA', *J. Nano Res.*, vol. 50, pp. 105–115, 2017, doi: 10.4028/www.scientific.net/JNanoR.50.105.

[2] I.U. Ibrahim, M. Sharifpur, J.P. Meyer, S.M.S. Murshed, Experimental investigations of nanoparticle size effects on force convective heat transfer characteristics of Al2O3 - MWCNT hybrid nanofluids in transitional flow regime, International Journal of Heat and Mass Transfer, Vol. 228,2024,125597,ISSN 0017-9310, https://doi.org/10.1016/j.ijheatmasstransfer.2024.125597.

[3] S. Suseel Jai Krishnan, M. Momin, C. Nwaokocha, M. Sharifpur, and J. P. Meyer, "An empirical study on the persuasive particle size effects over the multi-physical properties of monophase MWCNT-Al2O3 hybridized nanofluids," *J Mol Liq*, vol. 361.

[4] S. Suresh, K.P. Venkitaraj, P. SSelvakumar, M. Chandrasekar, "Effect of Al2O3–Cu/water hybrid nanofluid in heat transfer," *Exp Therm Fluid Sci*, vol. 38, pp. 54–60, Apr. 2012, doi: 10.1016/J.EXPTHERMFLUSCI.2011.11.007.

[5] K.A. Hamid, W.H. Azmi, M.F. Nabil, R. Mamat, Experimental investigation of nanoparticle mixture ratios on TiO2–SiO2 nanofluids heat transfer performance under turbulent flow, Int J Heat Mass Transf 118 (Mar. 2018) 617–627, https://doi.org/10.1016/j.ijheatmasstransfer.2017.11.036.

[6] M.H. Ahmadi, A. Mirlohi, M. Alhuyi Nazari, R. Ghasempour, A review of thermal conductivity of various nanofluids, J Mol Liq 265 (2018) 181–188, https://doi.org/10.1016/j.molliq.2018.05.124.

[7] S. Nallusamy, A. Manoj Babu, X-Ray differaction and fesem analysis for mixture of hybrid nano particles in heat transfer applications, J. Nano Res. 37 (2016) 58–67, https://doi.org/10.4028/www.scientific.net/JNanoR.37.58.

[8] A. Hussien, M.Z. Abdullah, N.M. Yusop, M.A. Al-Nimr, M.A. Atieh, M. Mehrali, Experiment on forced convective heat transfer enhancement using MWCNTs/GNPs hybrid nanofluid and mini-tube, Int J Heat Mass Transf 115 (2017) 1121–1131, https://doi.org/10.1016/j.ijheatmasstransfer.2017.08.120.

[9] S.O. Giwa, M. Momin, C.N. Nwaokocha, M. Sharifpur, J.P. Meyer, Influence of nanoparticles size, percent mass ratio, and temperature on the thermal properties of water-based MgO–ZnO nanofluid: an experimental approach, J Therm Anal Calorim 143 (2) (Jan. 2021) 1063–1079, https://doi.org/10.1007/S10973-020-09870-X/FIGURES/23.

[10] M. Shahul Hameed, S. Suresh, R.K. Singh, "Comparative study of heat transfer and friction characteristics of water-based Alumina–copper and Alumina–CNT hybrid nanofluids in laminar flow through pipes," *J Therm Anal Calorim*, vol. 136, no. 1, pp. 243–253, Apr. 2019, Doi: 10.1007/s10973-018-7898-z.

[11] M. Shahul Hameed, S. Suresh, "Convective heat transfer and pressure drop characteristics of Al2O3-CNT/water hybrid nanofluid in a straight circular tube under turbulent flow," Journal of Nanofluids, vol. 6, no. 4, pp. 743–750, Aug. 2017, Doi: 10.1166/jon.2017.1370.

[12] J.P. Meyer, in: Heat transfer in tubes in the transitional flow regime, Begell House Inc., 2014, https://doi.org/10.1615/ihtc15.kn.000003.

[13] M. Everts, P. Robbertse, B. Spitholt, The effects of surface roughness on fully developed laminar and transitional flow friction factors and heat transfer coefficients in horizontal circular tubes, Int J Heat Mass Transf 189 (Jun. 2022) 122724, https://doi.org/10.1016/J.IJHEATMASSTRANSFER.2022.122724.

[14] J. Ghajar, K.F. Madon, Pressure drop measurements in the transition region for a circular tube with three different inlet configurations, Exp Therm Fluid Sci 5 (1) (Jan. 1992) 129–135, https://doi.org/10.1016/0894-1777(92)90062-A.

[15] J.P. Meyer, T.J. McKrell, K. Grote, The influence of multi-walled carbon nanotubes on single-phase heat transfer and pressure drop characteristics in the transitional flow regime of smooth tubes, Int J Heat Mass Transf 58 (1–2) (2013) 597–609, https://doi.org/10.1016/j.ijheatmasstransfer.2012.11.074.

[16] S.S. Chougule, S.K. Sahu, Comparative Study on Heat Transfer Enhancement of Low Volume Concentration of Al2o3-Water and Carbon Nano-Tube-Water Nano-Fluids in Transition Regime Using Helical Screw Tape Inserts, Experimental Heat Transfer 29 (1) (2016) 17–36, https://doi.org/10.1080/08916152.2014.926432.

[17] S. Osman, M. Sharifpur, J.P. Meyer, Experimental investigation of convection heat transfer in the transition flow regime of aluminium oxide-water nanofluids in a rectangular channel, Int J Heat Mass Transf 133 (2019) 895–902, https://doi.org/10.1016/j.ijheatmasstransfer.2018.12.169.

[18] K.V. Sharma, L.S. Sundar, P.K. Sarma, Estimation of heat transfer coefficient and friction factor in the transition flow with low volume concentration of Al2O3 nanofluid flowing in a circular tube and with twisted tape insert, International Communications in Heat and Mass Transfer 36 (5) (2009) 503–507, https://doi.org/10.1016/j.icheatmasstransfer.2009.02.011.

[19] Y. Yang, Z.G. Zhang, E.A. Grulke, W.B. Anderson, G. Wu, Heat transfer properties of nanoparticle-in-fluid dispersions (nanofluids) in laminar flow, Int J Heat Mass Transf 48 (6) (2005) 1107–1116, https://doi.org/10.1016/j.ijheatmasstransfer.2004.09.038.

[20] J. Ma, Y. Xu, W. Li, J. Zhao, S. Zhang, S. Basov, Experimental Investigation into the Forced Convective Heat Transfer of Aqueous Fe 3 O 4 Nanofluids under Transition Region, Journal of Nanoparticles 2013 (2013) 1–5, https://doi.org/10.1155/2013/601363.

[21] M.T. Naik, L.S. Sundar, Heat Transfer and Friction Factor with Water/Propylene Glycol-Based CuO Nanofluid in Circular Tube with Helical Inserts under Transition Flow Regime, Heat Transfer Engineering 35 (1) (2014) 53–62, https://doi.org/10.1080/01457632.2013.810451.

[22] Y.S. Chen, H.H. Zhu, J. Tian, Y. Fu, Z.F. Tang, N.X. Wang, Convective heat transfer characteristics in the laminar and transition region of molten salt in concentric tube, Appl Therm Eng 117 (May 2017) 682–688, https://doi.org/10.1016/J.APPLTHERMALENG.2017.01.070.

[23] W. Li, Z.Z. Feng, Laminar mixed convection of large-Prandtl-number in-tube nanofluid flow, Part II: Correlations, Int J Heat Mass Transf 65 (Jan. 2013) 928–935, https://doi.org/10.1016/J.IJHEATMASSTRANSFER.2013.07.006.

[24] D.R. Oliver, The effect of natural convection on viscous-flow heat transfer in horizontal tubes, Chem Eng Sci 17 (5) (1962) 335–350, https://doi.org/10.1016/0009-2509(62)80035-9.

[25] E. Bergles, "experimental verification of analyses and correlation of the effects of temperature-dependent fluid properties on laminar heat transfers." Pp. 473–486, 1983.

[26] G.S. Barozzi, E. Zanchini, M. Mariotti, Experimental investigation of combined forced and free convection in horizontal and inclined tubes, Meccanica 20 (1) (Mar. 1985) 18–27, https://doi.org/10.1007/BF02337057.

[27] B. Shome, M.K. Jensen, Mixed convection laminar flow and heat transfer of liquids in isothermal horizontal circular ducts, Int J Heat Mass Transf 38 (11) (Jul. 1995) 1945–1956, https://doi.org/10.1016/0017-9310(94)00328-S.

[28] N. Kumar, S.S. Sonawane, S.H. Sonawane, Experimental study of thermal conductivity, heat transfer and friction factor of Al2O3 based nanofluid, International Communications in Heat and Mass Transfer 90 (Jan. 2018) 1–10, https://doi.org/10.1016/j.icheatmasstransfer.2017.10.001.

[29] Z.Z. Feng, W. Li, Laminar mixed convection of large-Prandtl-number in-tube nanofluid flow, Part I: Experimental study, Int J Heat Mass Transf 65 (Oct. 2013) 919–927, https://doi.org/10.1016/J.IJHEATMASSTRANSFER.2013.07.005.

[30] M. Mahbubul, R. Saidur, M.A. Amalina, Latest developments on the viscosity of nanofluids, Int J Heat Mass Transf 55 (4) (Jan. 2012) 874–885, https://doi.org/10.1016/J.IJHEATMASSTRANSFER.2011.10.021.

[31] R. Prasher, D. Song, J. Wang, A. Advances, Measurements of nanofluid viscosity and its implications for thermal applications Articles You May Be Interested In

[32] P.K. Namburu, D.P. Kulkarni, D. Misra, D.K. Das, Viscosity of copper oxide nanoparticles dispersed in ethylene glycol and water mixture, Exp Therm Fluid Sci 32 (2) (Nov. 2007) 397–402, https://doi.org/10.1016/J.EXPTHERMFLUSCI.2007.05.001.

[33] H. Chen, S. Witharana, Y. Jin, C. Kim, Y. Ding, Predicting thermal conductivity of liquid suspensions of nanoparticles (nanofluids) based on rheology, Particuology 7 (2) (Apr. 2009) 151–157, https://doi.org/10.1016/J.PARTIC.2009.01.005.

[34] H. Zhu, C. Li, D. Wu, C. Zhang, Y. Yin, Preparation, characterization, viscosity and thermal conductivity of CaCO3 aqueous nanofluids, Sci China Technol Sci 53 (2) (Feb. 2010) 360–368, https://doi.org/10.1007/S11431-010-0032-5/METRICS.

[35] M.M. Derakhshan, M.A. Akhavan-Behabadi, Mixed convection of MWCNT–heat transfer oil nanofluid inside inclined plain and microfin tubes under laminar assisted flow, International Journal of Thermal Sciences 99 (Jan. 2016) 1–8, https://doi.org/10.1016/J.IJTHERMALSCI.2015.07.025.

[36] R. Ben Mansour, N. Galanis, C.T. Nguyen, "Experimental study of mixed convection with water–Al2O3 nanofluid in inclined tube with uniform wall heat flux," *International Journal of Thermal Sciences*, vol. 50, no. 3, pp. 403–410, Mar. 2011, doi: 10.1016/J.IJTHERMALSCI.2010.03.016.

[37] R. Ben Mansour, N. Galanis, C.T. Nguyen, "Developing laminar mixed convection of nanofluids in an inclined tube with uniform wall heat flux," *Int J Numer Methods Heat Fluid Flow*, vol. 19, no. 2, pp. 146–164, Mar. 2009, doi: 10.1108/09615530910930946/FULL/PDF.

[38] K. Khanafer, K. Vafai, M. Lightstone, Buoyancy-driven heat transfer enhancement in a two-dimensional enclosure utilizing nanofluids, Int J Heat Mass Transf 46 (19) (Sep. 2003) 3639–3653, https://doi.org/10.1016/S0017-9310(03)00156-X.

[39] R. Ben Mansour, N. Galanis, C.T. Nguyen, C. Aouina, "Experimental Study of Mixed Convection Laminar Flow of Water-Al 2 O 3 Nanofluid in Horizontal Tube with Uniform Wall Heat Flux".

[40] E. Manay, Emre Mandev, E. Mandev, "Experimental investigation of mixed convection heat transfer of nanofluids in a circular microchannel with different inclination angles," *J Therm Anal Calorim*, vol. 135, doi: 10.1007/s10973-018-7463-9.

[41] L.S. Sundar, A.C.M. Sousa, M.K. Singh, "Heat transfer enhancement of low volume concentration of carbon nanotube-Fe3O4/water hybrid nanofluids in a tube with twisted tape inserts under turbulent flow," *J Therm Sci Eng Appl*, vol. 7, no. 2, 2015, doi: 10.1115/1.4029622.

[42] T. Balaji, S. Rajendiran, C. Selvam, D.M. Lal, Enhanced heat transfer characteristics of water based hybrid nanofluids with graphene nanoplatelets and multi walled carbon nanotubes, Powder Technol 394 (Dec. 2021) 1141–1157, https://doi.org/10.1016/j.powtec.2021.09.014.

[43] Shahsavar, M. Saghafian, M.R. Salimpour, M.B. Shafii, "Experimental investigation on laminar forced convective heat transfer of ferrofluid loaded with carbon nanotubes under constant and alternating magnetic fields," *Exp Therm Fluid Sci*, vol. 76, pp. 1–11, Sep. 2016, doi: 10.1016/j.expthermflusci.2016.03.010.

[44] M. Gupta, V. Singh, Z. Said, Heat transfer analysis using zinc Ferrite/water (Hybrid) nanofluids in a circular tube: An experimental investigation and development of new correlations for thermophysical and heat transfer properties, Sustainable Energy Technologies and Assessments 39 (Jun. 2020), https://doi.org/10.1016/j.seta.2020.100720.

[45] Naddaf, S. Zeinali Heris, B. Pouladi, "An experimental study on heat transfer performance and pressure drop of nanofluids using graphene and multi-walled carbon nanotubes based on diesel oil," *Powder Technol*, vol. 352, pp. 369–380, Jun. 2019, doi: 10.1016/j.powtec.2019.04.078.

[46] A. Hussien, M.Z. Abdullah, N.M. Yusop, W. Al-Kouz, E. Mahmoudi, M. Mehrali, "Heat transfer and entropy generation abilities of MWCNTs/GNPs hybrid nanofluids in microtubes," *Entropy*, vol. 21, no. 5, May 2019, doi: 10.3390/e21050480.

[47] L. Megatif, A. Ghozatloo, A. Arimi, M. Shariati-Niasar, Investigation of Laminar Convective Heat Transfer of a Novel Tio2-Carbon Nanotube Hybrid Water-Based Nanofluid, Experimental Heat Transfer 29 (1) (Jan. 2016) 124–138, https://doi.org/10.1080/08916152.2014.973974.

[48] M. Gupta, V. Singh, S. Kumar, N. Dilbaghi, Experimental analysis of heat transfer behavior of silver, MWCNT and hybrid (silver +MWCNT) nanofluids in a laminar tubular flow, J Therm Anal Calorim 142 (4) (Nov. 2020) 1545–1559, https://doi.org/10.1007/s10973-020-09453-w.

[49] M.H. Aghabozorg, A. Rashidi, S. Mohammadi, Experimental investigation of heat transfer enhancement of Fe2O3-CNT/water magnetic nanofluids under laminar, transient and turbulent flow inside a horizontal shell and tube heat exchanger, Exp Therm Fluid Sci 72 (2016) 182–189, https://doi.org/10.1016/j.expthermflusci.2015.11.011.

[50] J.P. Meyer, M. Everts, Single-phase mixed convection of developing and fully developed flow in smooth horizontal circular tubes in the laminar and transitional flow regimes, Int J Heat Mass Transf 117 (Feb. 2018) 1251–1273, https://doi.org/10.1016/J.IJHEATMASSTRANSFER.2017.10.070.

[51] J. Ghajar, L.M. Tam, Heat transfer measurements and correlations in the transition region for a circular tube with three different inlet configurations, Exp Therm Fluid Sci 8 (1) (Jan. 1994) 79–90, https://doi.org/10.1016/0894-1777(94)90075-2.

[52] Y. Li, J. Zhou, S. Tung, E. Schneider, S. Xi, A review on development of nanofluid preparation and characterization, Powder Technol 196 (2) (Dec. 2009) 89–101, https://doi.org/10.1016/J.POWTEC.2009.07.025.

[53] K.B. Anoop, T. Sundararajan, S.K. Das, Effect of particle size on the convective heat transfer in nanofluid in the developing region, Int J Heat Mass Transf 52 (9–10)

(Apr. 2009) 2189–2195, https://doi.org/10.1016/j.
ijheatmasstransfer.2007.11.063.

[54] Ahmadi Nadooshan, H. Eshgarf, M. Afrand, "Measuring the viscosity of Fe3O4-
MWCNTs/EG hybrid nanofluid for evaluation of thermal efficiency: Newtonian and
non-Newtonian behavior," *J Mol Liq*, vol. 253, pp. 169–177, Mar. 2018, doi:
10.1016/J.MOLLIQ.2018.01.012.

[55] L.S. Sundar, M.K. Singh, A.C.M. Sousa, Enhanced heat transfer and friction factor of
MWCNT-Fe3O4/water hybrid nanofluids, International Communications in Heat
and Mass Transfer 52 (Mar. 2014) 73–83, https://doi.org/10.1016/j.
icheatmasstransfer.2014.01.012.

[56] U. Ibrahim, M. Sharifpur, J.P. Meyer, Experimental investigations of particle sizes
effects on exergy and entropy characteristics of AL2O3 - MWCNT hybrid nanofluid
along the transitional flow regime, Case Studies in Thermal Engineering 51 (Nov.
2023) 103575, https://doi.org/10.1016/J.CSITE.2023.103575.

[57] S.O. Giwa, M. Sharifpur, M.H. Ahmadi, J.P. Meyer,
"Experimental Investigation on Stability, Viscosity, and Electrical Conductivity of
Water-Based Hybrid Nanofluid of MWCNT-Fe2O3," *Nanomaterials 2021, Vol. 11,
Page 136*, vol. 11, no. 1, p. 136, Jan. 2021, doi: 10.3390/NANO11010136.

[58] S.O. Giwa, M. Sharifpur, J.P. Meyer, S. Wongwises, O. Mahian, Experimental
measurement of viscosity and electrical conductivity of water-based γ-Al2O3/
MWCNT hybrid nanofluids with various particle mass ratios, J Therm Anal Calorim
143 (2) (2021) 1037–1050, https://doi.org/10.1007/s10973-020-10041-1.

[59] F. Durst, S. Ray, B. Ünsal, O.A. Bayoumi, The development lengths of laminar pipe
and channel flows, Journal of Fluids Engineering, Transactions of the ASME 127
(6) (Nov. 2005) 1154–1160, https://doi.org/10.1115/1.2063088.

[60] S.I. Abu-Eishah, Correlations for the Thermal Conductivity of Metals as, Int J
Thermophys 22 (6) (2001) 1855–1868.

[61] O. Popiel, J. Wojtkowiak, Simple formulas for thermophysical properties of liquid
water for heat transfer calculations (from 0°c to 150°c), Heat Transfer Engineering
19 (3) (1998) 87–101, https://doi.org/10.1080/01457639808939929.

[62] Choon pak and y. I. Cho, "experimental heat transfer an international journal
hydrodynamic and heat transfer study of dispersed fluids with submicron metallic
oxide particles," 2007, doi: 10.1080/08916159808946559.

[63] A. Depew, S.E. August, Heat Transfer Due to Combined Free and Forced
Convection in a Horizontal and Isothermal Tube, J Heat Transfer 93 (4) (Nov.
1971) 380–384, https://doi.org/10.1115/1.3449834.

[64] R. Brown, M.A. Thomas, Combined Free and Forced Convection Heat Transfer for
Laminar Flow in Horizontal Tubes, Journal of Mechanical Engineering Science 7
(4) (Dec. 1965) 440–448, https://doi.org/10.1243/JMES_JOUR_1965_007_066_02.

[65] J.G. Yunus, A. Cengal, "Heat and Mass Trasnfer: Fundametals and Applications,"
Heat and Mass Trasnfer: Fundametals and Applications, vol. 1, pp. 67–142, 379–424,
2014, Accessed: Jun. 09, 2023. [Online]. Available: https://books.google.com/
books/about/Heat_and_Mass_Transfer_Fundamentals_and.html?
id=B89MnwEACAAJ.

[66] P. Dunn, M. Davis, *Measurement and data analysis for engineering and science*. 2017.
Accessed: Oct. 07, 2023. [Online]. Available: https://books.google.com/books?
hl=en&lr=&id=bmlQDwAAQBAJ&oi=fnd&pg=PP1&ots=H0LAUUIWz2&sig=
Mi44eXrMD0KQ0w6qWH3ns-48R7o.

[67] H.K. Tam, L.M. Tam, A.J. Ghajar, Effect of inlet geometries and heating on the
entrance and fully-developed friction factors in the laminar and transition regions
of a horizontal tube, Exp Therm Fluid Sci 44 (2013) 680–696, https://doi.org/
10.1016/j.expthermflusci.2012.09.008.

[68] P. Meyer, J.A. Olivier, Transitional flow inside enhanced tubes for fully developed
and developing flow with different types of inlet disturbances: Part I - Adiabatic
pressure drops, Int J Heat Mass Transf 54 (7–8) (Mar. 2011) 1587–1597, https://
doi.org/10.1016/j.ijheatmasstransfer.2010.11.027.

[69] H.R. Nagendra, Interaction of free and forced convection in horizontal tubes in the
transition regime, J Fluid Mech 57 (2) (1973) 269–288, https://doi.org/10.1017/
S0022112073001151.

[70] J. Ghajar, L.-M. Tam, "Heat Transfer Measurements and Correlations in the
Transition Region for a Circular Tube with Three Different Inlet, Configurations"
(1994).

[71] M. Everts, J.P. Meyer, Heat transfer of developing and fully developed flow in
smooth horizontal tubes in the transitional flow regime, Int J Heat Mass Transf 117
(Feb. 2018) 1331–1351, https://doi.org/10.1016/J.
IJHEATMASSTRANSFER.2017.10.071.

[72] Andrade, A.S. Moita, A. Nikulin, A.L.N. Moreira, H. Santos, "Experimental
investigation on heat transfer and pressure drop of internal flow in corrugated
tubes," *Int J Heat Mass Transf*, vol. 140, pp. 940–955, Sep. 2019, doi: 10.1016/J.
IJHEATMASSTRANSFER.2019.06.025.

[73] M. Everts and J.P. Meyer, "Flow Regime Maps for Fully Developed Flow in
Horizontal Solar Receiver Tubes".Int. J. Heat Mass Transf., Vol. 117, pp.1274-
1290, 2018.

[74] P. Abraham, E.M. Sparrow, W.J. Minkowycz, "Internal-flow Nusselt numbers for
the low-Reynolds-number end of the laminar-to-turbulent transition regime", doi:
10.1016/j.ijheatmasstransfer.2010.09.012.